

Methane Pyrolysis for Zero-Emission Hydrogen Production: A Potential Bridge Technology from Fossil Fuels to a Renewable and Sustainable Hydrogen Economy

Nuria Sánchez-Bastardo,* Robert Schlögl, and Holger Ruland*

Cite This: *Ind. Eng. Chem. Res.* 2021, 60, 11855–11881

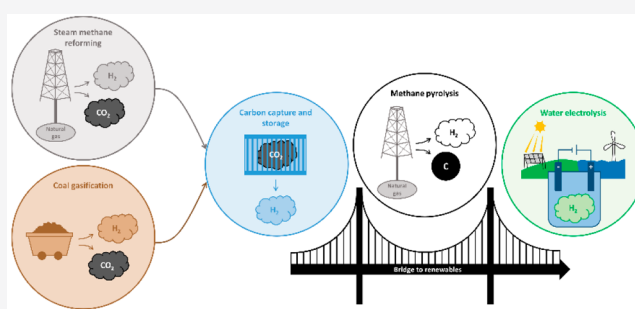
Read Online

ACCESS |

Metrics & More

Article Recommendations

ABSTRACT: Hydrogen plays a key role in many industrial applications and is currently seen as one of the most promising energy vectors. Many efforts are being made to produce hydrogen with zero CO₂ footprint via water electrolysis powered by renewable energies. Nevertheless, the use of fossil fuels is essential in the short term. The conventional coal gasification and steam methane reforming processes for hydrogen production are undesirable due to the huge CO₂ emissions. A cleaner technology based on natural gas that has received special attention in recent years is methane pyrolysis. The thermal decomposition of methane gives rise to hydrogen and solid carbon, and thus, the release of greenhouse gases is prevented. Therefore, methane pyrolysis is a CO₂-free technology that can serve as a bridge from fossil fuels to renewable energies.



1. INTRODUCTION

The establishment of a sustainable power system to meet the growing energy demand is one of our most critical current challenges. The basis of this energy system is the decrease of greenhouse gas (GHG) emissions to reduce global warming, and thus, accomplish the goals set out in the Paris Agreement¹ and Kyoto Protocol.² Specifically, Germany aims to become carbon neutral by 2050.³ Since most CO₂ emissions derive from the combustion of fossil fuels for power generation, much research is concerned at present with the development of zero-emission fuels.⁴ The hydrogen economy concept is based on the use of hydrogen as a potential fuel.⁵ Hydrogen is one of the most promising energy carriers and is considered the cleanest fuel because its combustion produces only water.⁶ In addition to this, the combustion of hydrogen originates more energy on a mass basis than conventional fossil fuels.^{7,8} Hydrogen has received special attention for its application in fuel cells and internal combustion engines, enabling the creation of a low-carbon hydrogen economy.⁹ The chemical energy of hydrogen can be efficiently converted to electricity and other energy forms without GHG emissions.^{7,8,10,11} Hydrogen also plays a major role in the development of new strategies for converting industrial CO₂ emissions into important platform chemicals. This is actually one of the objectives set within the Carbon2Chem project, which aims to convert steel mill gases into base chemicals such as methanol.^{12,13} Thereby, the transformation of industrial emissions into chemicals prevents the release of GHG into the atmosphere.

Although hydrogen is a zero-emission fuel, its suitability also depends on the energy consumed and the cleanliness of the production method.¹⁴ The production of hydrogen via water electrolysis using electricity from renewable energies is the most appropriate technology from an environmental point of view due to its zero carbon footprint. The global consumption of renewables is predicted to grow in the next years, but will still remain relatively low for the foreseeable future (Figure 1).¹⁵ Drawbacks such as the fluctuations of renewable energies, geographic limitations, and problems related to energy storage have to be overcome.^{16,17} For instance, the available renewable energies in Germany, that is, onshore wind and solar energies, could provide electricity up to 2000 h a year, which is by far too less to deal with the annual power demand.¹⁸ Further electricity may be supplied by offshore wind energy, but the transportation from the coast to inland areas is still a problem today. Due to power fluctuations, energy-deficit periods will alternate with excess production seasons. The storage of power surplus could be a solution to the intermittence of renewable energy. However, large-scale energy storage remains a challenge.^{19,20}

Received: May 2, 2021
Revised: July 29, 2021
Accepted: July 29, 2021
Published: August 9, 2021



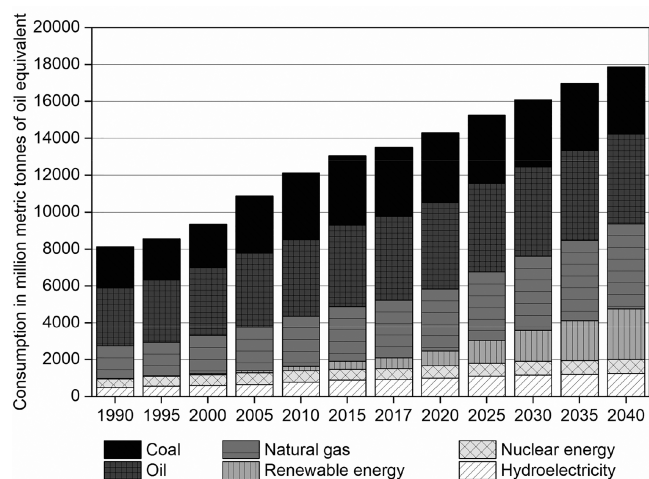


Figure 1. World energy consumption by energy source according to the data reported in ref 15.

Due to the large reserves of fossil fuels and the well-established technologies for their processing, fossil resources will still represent a major part of our energy system in the short term.^{7,21} For this reason, the development of bridge technologies based on fossil fuels with a low environmental impact has been the focus of countless studies in the last years. Among fossil fuels natural gas is currently the main source of hydrogen (48%) followed by oil (30%) and coal (18%), whereas only 4% of the global hydrogen production comes from renewable resources.⁸ Natural gas is expected to gain importance in the next few years over the use of oil and coal, the share of which within the total energy consumption will suffer a meaningful decline (Figure 1).²¹ Steam reforming and gasification of fossil fuels are currently the main processes for hydrogen production due to their technological maturity on an industrial scale. Nevertheless, the major drawback is the unavoidable generation of large amounts of GHGs.²²

Unlike these fossil fuel-based technologies, the pyrolysis of methane appears as a potential process for the transition to a sustainable hydrogen economy.²¹ Methane pyrolysis involves the thermal decomposition of methane into its components, that is, hydrogen and carbon. Therefore, the greatest benefit is the generation of CO₂-free hydrogen with solid carbon as the only byproduct. This is a unique advantage of methane pyrolysis over the conventional steam methane reforming (SMR) and coal gasification processes. Depending on the characteristics and price of the carbon product, its sale may improve the economics of the industrial methane pyrolysis process.^{9,21,23–26} Here, the main problem is the absence of markets that can accommodate such large amounts of carbon, and hence, new applications become necessary.^{9,23} The use of carbon for soil amendment and environmental remediation may be the only alternative that would offer a huge market for the carbon resulting from methane pyrolysis.^{27,28} However, further studies are needed to prove the suitability of the pyrolysis carbon for such an application.²⁷ On the other hand, if carbon is to be stored, the costs associated with solid carbon storage would be lower than the sequestration of CO₂ derived from SMR.²⁹ Owing to the depletion of natural gas, the production of hydrogen via methane pyrolysis is not a sustainable process in the long term. Nevertheless, it may be a temporary solution and probably the most cost-effective bridging technology over the transition period toward

renewable energies.²⁶ This review aims to provide a comprehensive and critical overview of methane pyrolysis with a focus on industrial application. Crucial aspects for the industrialization of the process, such as the use of suitable catalysts and the implementation of feasible processes on an industrial scale, or the finding of realistic applications for the carbon product, are thoroughly discussed in this review.

2. TRADITIONAL AND DEVELOPING TECHNOLOGIES FOR HYDROGEN PRODUCTION

At present fossil fuels undoubtedly predominate over renewable resources for hydrogen production due to their high availability and cost-effective industrially implemented processes. About 96% of global hydrogen production is obtained by coal gasification, oil/naphtha reforming, and steam reforming of methane.²¹ However, these processes have a dramatic environmental impact owing to the large amount of CO₂ emissions. Coal gasification has the largest CO₂ footprint but also the lowest product costs. Because natural gas has a lower carbon content than coal, steam reforming of methane has a much smaller carbon footprint than coal gasification, although the product costs are slightly higher (Figure 2).³⁰

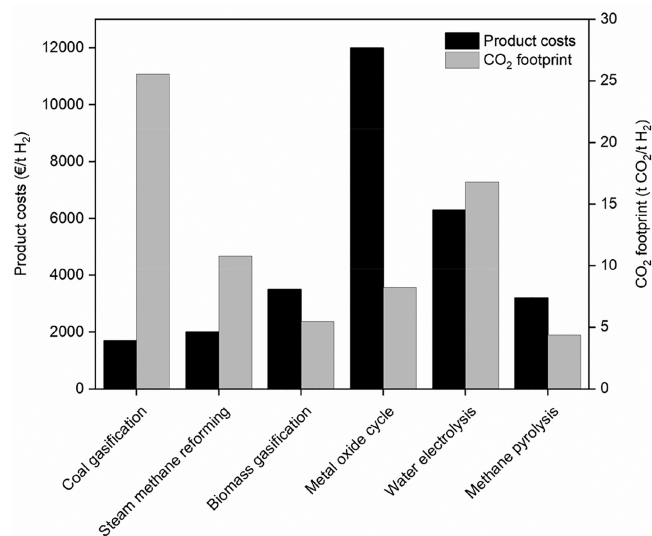


Figure 2. Product costs and CO₂ footprint of different hydrogen production technologies according to the data reported in ref 30. Note: The water electrolysis, metal oxide cycle and methane pyrolysis processes produce CO₂-free hydrogen. The CO₂ footprint of water electrolysis and the metal oxide cycle corresponds to the production of electricity from the grid. In the case of methane pyrolysis, in addition to the CO₂ emissions derived from the generation of electricity, those resulting from the extraction and transportation of natural gas are also taken into account.

SMR has a high energy efficiency (75%), but the need for carbon capture and storage (CCS) systems to obtain high purity hydrogen and decrease the GHG emissions results in a significant energy efficiency drop (60%) (Table 1),²⁸ and may increase the cost of hydrogen production more than 30%.³¹ In addition, the high electricity consumption of the conventional techniques intended for CCS increases the total environmental impact of the process.³² Dry methane reforming is an additional technology for hydrogen production using natural gas as a feedstock. This process generates less CO₂ emissions than SMR, but it is highly endothermic and is generally

Table 1. Energy Efficiencies of Different Technologies for Hydrogen Production

technology	energy efficiency in transformation (%)	energy efficiency with CCS (%)	ref
coal gasification	60	43	22
steam methane reforming	75	60	28
biomass gasification	35–50		40
thermochemical water splitting	20–45		41
water electrolysis	50–70		40
methane pyrolysis	58	58	28

intended for the production of syngas, rather than for pure hydrogen, suitable for the synthesis of higher hydrocarbons and oxygenated derivatives.³³ Biomass gasification is a mature technology that converts biomass into a hydrogen containing gas mixture. Although biomass is considered as a renewable raw material, its limited availability and the complex logistics for transportation to decentralized industries are factors that affect negatively its applicability and the final product costs.³⁰ Moreover, the production of hydrogen is accompanied by significant amounts of CO₂ that force the implementation of further separation and purification steps.⁶ For this reason, biomass gasification is usually intended for direct syngas production to generate energy or synthesize fuels rather than for obtaining pure hydrogen.³⁴

A great effort is being made to establish industrial strategies for hydrogen production with near-zero CO₂ emissions. Thermochemical water splitting and water electrolysis are developing technologies that generate only hydrogen and oxygen. The most common thermochemical water splitting process consists of redox-active metal oxide cycles, which require high temperatures (>1300 °C) that can be achieved by large-scale sunlight concentration systems.³⁵ This technology uses two practically inexhaustible sources, namely water and sun. However, according to the economic evaluation of different hydrogen production processes on a large scale, the metal oxide cycle has the highest product costs and requires a high level of investment (Figure 2).³⁰ The integration of solar energy concentration systems with structures able to split water represents an extensive value and impact on the energy and economy. Nowadays this process is not industrially feasible owing to its relatively poor efficiency and high processing costs.⁶ Water electrolysis involves the decomposition of water into oxygen and hydrogen by passing an electric current.^{36,37} Hydrogen production from water via electrolysis is a completely CO₂-free alternative only if the required electricity comes exclusively from renewable resources.³⁰ If the electricity is not 100% emission-free, water electrolysis can even exceed the carbon footprint of SMR due to the high energy requirements.³⁸ The problems related to renewable energies, such as solar and wind, are their variability and unpredictability, which leads to difficulties to match energy supply and demand. The storage of energy during periods with power surplus is often seen as a crucial element of future power systems, but it is unlikely to be a universal solution for all demand–supply imbalance problems.³⁹ In the specific case of Germany, it seems improbable that a total dependence on renewable energy will be achieved. Thus, due to the high electricity consumption, the viability of water electrolysis depends on the price and carbon footprint of the required electricity.³⁰ Both water processing technologies are still not

economically competitive with the use of fossil fuels.^{7,26} They show the highest product costs, whereas the well-developed technologies, such as steam methane reforming and coal gasification, display the lowest product costs (Figure 2). Until the use of renewable energies is sufficiently expanded, processes based on fossil resources seem to be fundamental, and thus, cleaner economic technologies need to be developed and implemented industrially.

Methane, which is the main component of natural gas, is a suitable raw material in terms of availability due to the existence of huge natural gas reserves.⁶ Since SMR leads to significant CO₂ emissions, cleaner processes have to be investigated. The thermal decomposition of methane, also known as methane pyrolysis, is an adequate alternative because hydrogen and solid carbon are the only reaction products, and thus, the formation of CO₂ is prevented during the reaction itself.^{7,9} The CO₂ footprint of methane pyrolysis (Figure 2) corresponds to the emissions derived from the required electricity and those generated during the extraction and transportation of natural gas. In any case, the CO₂ emissions corresponding to methane pyrolysis are significantly lower than those derived from the well-established fossil fuel-based technologies.³⁰ Methane pyrolysis is a one-step process,⁹ unlike SMR in which the water–gas shift (WGS) reaction has to be carried out additionally. Via the WGS reaction the CO produced in the reaction between methane and water is converted into CO₂ and additional hydrogen.^{26,38} Regarding the energy efficiency, if the sequestration of CO₂ is not considered, SMR is significantly more efficient than methane pyrolysis (75% vs 58%). However, when the implementation of CCS systems is taken into account, the net energy efficiency of both processes becomes very similar (60% for SMR and 58% for methane pyrolysis).²⁸ Methane pyrolysis is more advantageous concerning the energy input requirement as well (Figure 3). According to the standard reaction enthalpies, 37.7 kJ are needed in methane pyrolysis to obtain one mole of H₂,^{7,42} whereas in SMR coupled with the water–gas shift reaction and without taking into account the heat for water evaporation this value amounts to 41.4 kJ per mole of H₂.⁴³ Nevertheless, if the heat required to evaporate liquid water is considered, then 63.4 kJ must be applied for the production of one mole of hydrogen in the steam reforming process.⁴³ The decomposition of methane is also energetically much more favorable than water electrolysis, where 285.8 kJ are required to produce one mole of hydrogen.³⁰ Despite the advantages of methane pyrolysis, the production of hydrogen from this process is not yet competitive with the mature steam reforming technology. The estimated product costs from the decomposition of methane range from 2600 to 3200 € per ton of hydrogen depending on the expected carbon credit. In contrast, one ton of hydrogen generated by steam reforming costs 2000 €. ³⁰ However, this value could increase in the future if higher penalties for CO₂ emissions are imposed. Although methane pyrolysis cannot compete economically today with the traditional process, and even though natural gas is a fossil raw material, this technology seems to be an appropriate temporary alternative for CO₂-free hydrogen production that can serve as a bridge in a transition period toward renewable energies.

3. REACTION MECHANISM OF METHANE PYROLYSIS

3.1. Reaction Mechanism of Noncatalytic Methane Pyrolysis. Different reaction mechanisms for the noncatalytic decomposition of methane have been postulated since the

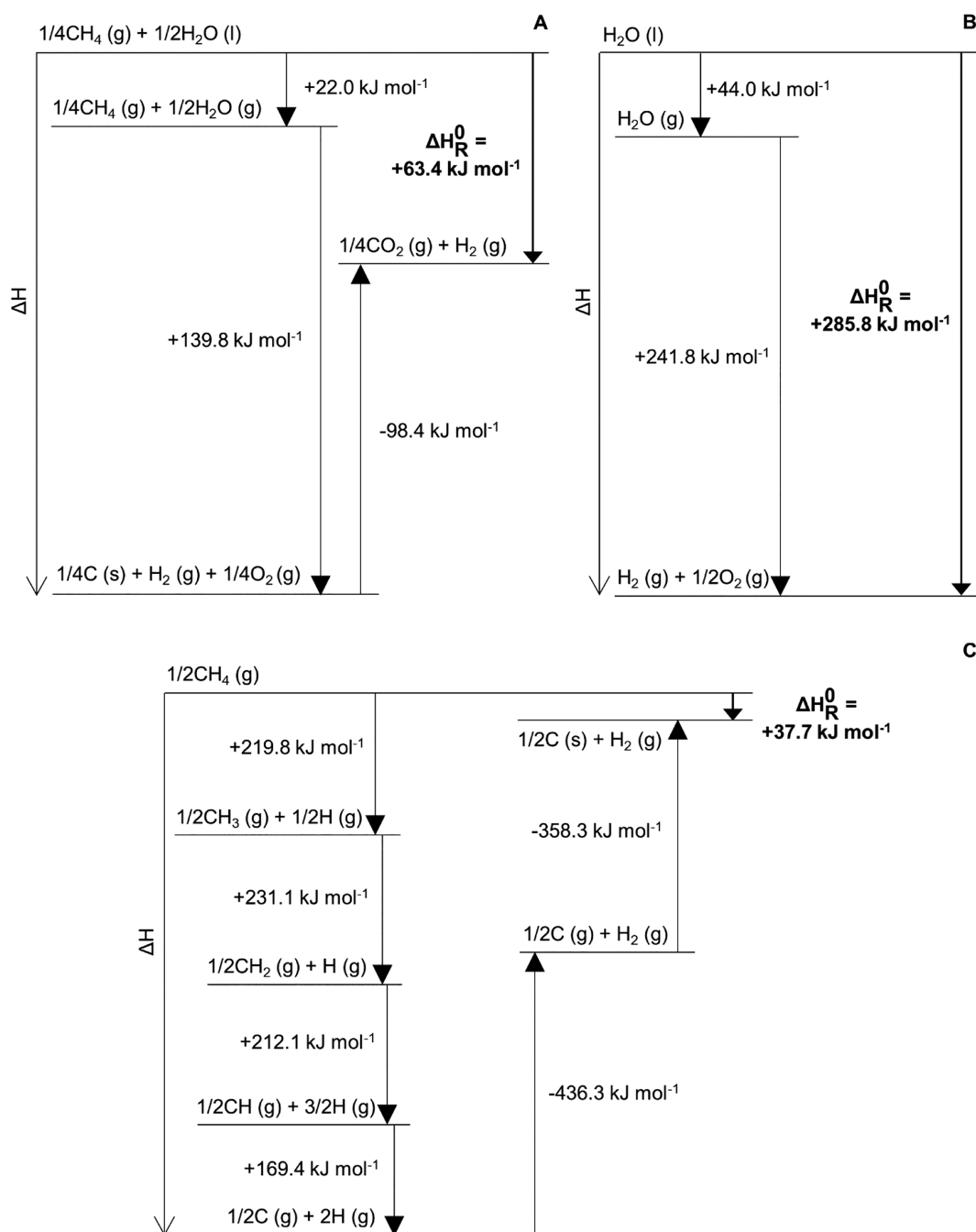
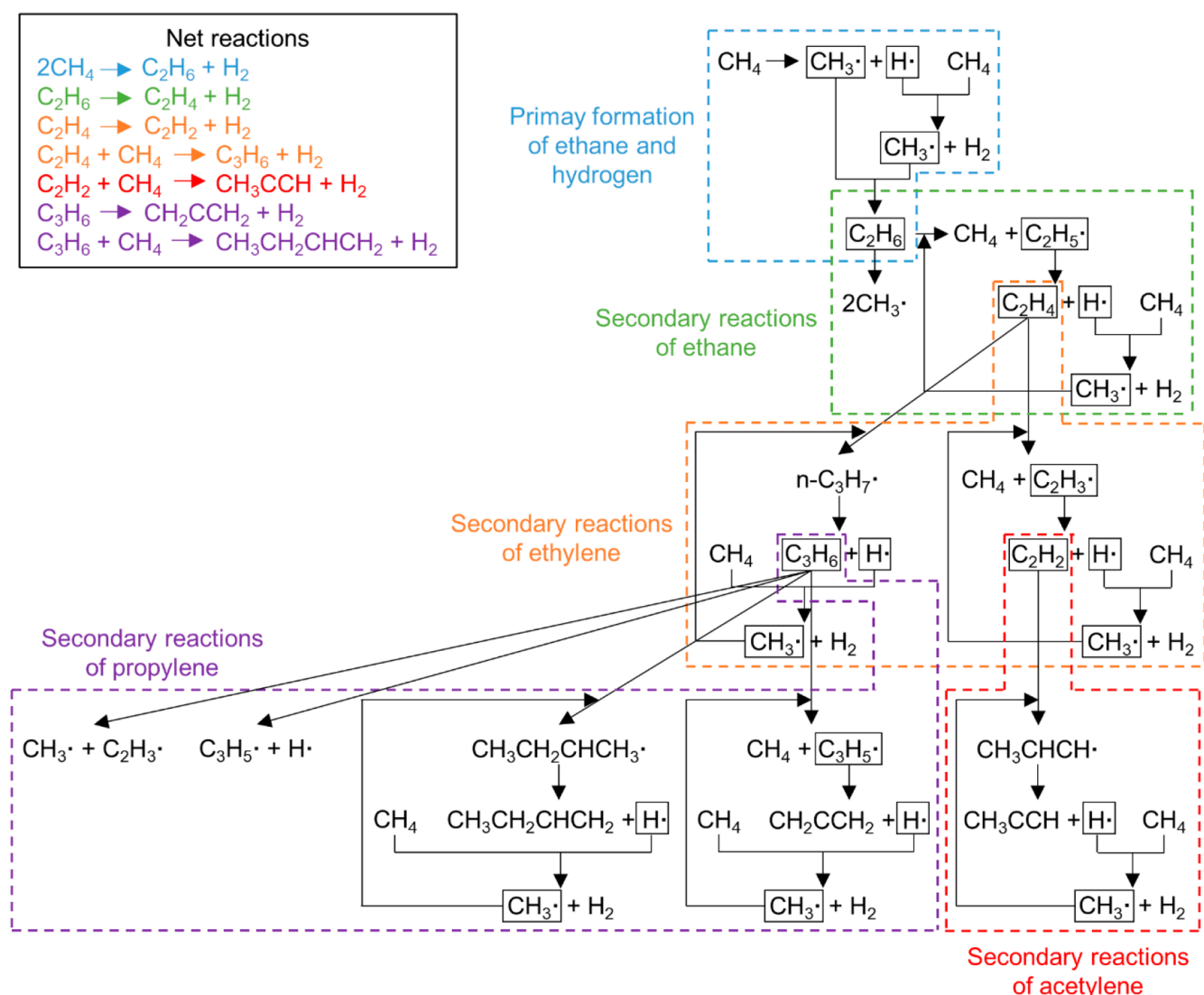


Figure 3. Enthalpy diagrams of (A) steam methane reforming, (B) water electrolysis, and (C) methane pyrolysis. $\Delta_f H_{\text{gas}}^0(\text{H}_2\text{O}) = 241.8 \text{ kJ mol}^{-1}$; $\Delta_f H_{\text{liquid}}^0(\text{H}_2\text{O}) = 285.8 \text{ kJ mol}^{-1}$; $\Delta H_{\text{vap}}^0(\text{H}_2\text{O}) = \Delta_f H_{\text{liquid}}^0(\text{H}_2\text{O}) - \Delta_f H_{\text{gas}}^0(\text{H}_2\text{O})$; $\Delta_f H_{\text{gas}}^0(\text{CO}_2) = -393.5 \text{ kJ mol}^{-1}$; $\Delta H_{\text{dis}}^0(\text{CH}_3\text{-H}) = 439.6 \text{ kJ mol}^{-1}$; $\Delta H_{\text{dis}}^0(\text{CH}_2\text{-H}) = 462.2 \text{ kJ mol}^{-1}$; $\Delta H_{\text{dis}}^0(\text{CH-H}) = 424.1 \text{ kJ mol}^{-1}$; $\Delta H_{\text{dis}}^0(\text{C-H}) = 338.7 \text{ kJ mol}^{-1}$; $\Delta H_{\text{dis}}^0(\text{H-H}) = 436.3 \text{ kJ mol}^{-1}$; $\Delta H_{\text{sub}}^0(\text{C}) = 716.7 \text{ kJ mol}^{-1}$. All enthalpies are taken from the National Institute of Standards and Technology (NIST), except the dissociation enthalpies (ΔH_{dis}^0), which were taken from ref 44.

1960s. Pyrolysis tests in shock-tube experiments have allowed measurement of the initial rate of methane dissociation.^{45–49} Most authors agree that the reaction mechanism involves a free-radical scheme with the initiating reaction step corresponding to the dissociation of methane into a methyl radical and a hydrogen atom.^{45,48,50–56} A detailed reaction mechanism resulting from experiments at low temperatures (<830 °C) was proposed in 1976 (Scheme 1).^{53,54} This mechanism is based on the cleavage of C–H bonds and the consequent formation of methyl radicals. C_{2+} hydrocarbons are generated by the

reaction between CH_3 radicals and other intermediate hydrocarbon species. In the first step, methane splits into a methyl radical and a hydrogen atom to subsequently form ethane and hydrogen molecules. In the second step, the rate of ethane formation falls gradually toward a plateau, and ethylene is obtained as a secondary product via the radical chain dehydrogenation of ethane. In addition, under certain conditions ethane can be dissociated into two methyl radicals. In the third step, acetylene and propylene are formed from ethylene via radical chain dehydrogenation and radical chain

Scheme 1. Reaction Mechanism of the Noncatalytic Methane Pyrolysis Proposed by Chen et al.^{53,54}

methylation reactions, respectively. At the same time, a sharp increase in the formation rate of ethane is observed. This fact is not explained by the described reaction mechanism, and autocatalysis is apparently involved. Unlike other works, where autocatalysis is attributed to the formation of catalytically active carbon, in the present studies the appearance of new radical sources in the autocatalytic region, probably coming from acetylene and propylene, may be responsible for the increased formation rates of ethane and the corresponding products derived from it.^{53,54}

This mechanism was extended in 1985 by adding reverse, isomerization, and abstraction and addition reactions for radicals up to C_3 reacting with primary and secondary products up to C_3 .⁵⁵ The reaction between methane and a methyl radical to produce ethane was taken into account at higher temperatures ($>1000^\circ\text{C}$) (eq 1).^{45,56} Nevertheless, the formation of ethane is unlikely above 1000°C and the direct production of ethylene from methane is more probable (eqs 2 and 3). According to the same study, the formation of benzene occurs from acetylene (eq 4) and ethylene (eqs 5–7), and even if both hydrocarbons can form carbon directly, benzene

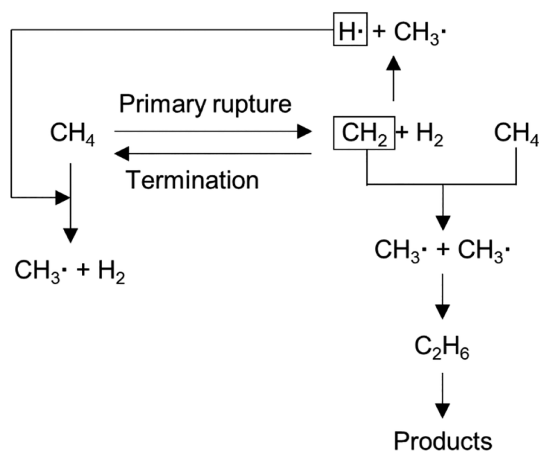
and probably higher condensed aromatics are the main species for carbon growth.⁵⁶



Although it is generally accepted that the rate-limiting step is the splitting of methane into a methyl radical and a hydrogen atom, another reaction mechanism with an alternative rate-determining step has also been proposed. In this case, the controlling stage corresponds to the dissociation of methane into methylene and a hydrogen molecule (Scheme 2):^{46,47}

These controversial results in the initiating and rate-controlling step may be related to the different temperature

Scheme 2. Reaction Mechanism of the Noncatalytic Methane Pyrolysis Proposed by Kevorkian et al.⁴⁶ and Kozlov and Knorre⁴⁷



ranges used in methane pyrolysis experiments. The decomposition of methane into a methyl radical and a hydrogen atom is observed in experiments at lower temperatures (<1400 °C), whereas the dissociation into methylene and a hydrogen molecule derives from reactions at higher temperatures (>1400 °C).⁵⁷

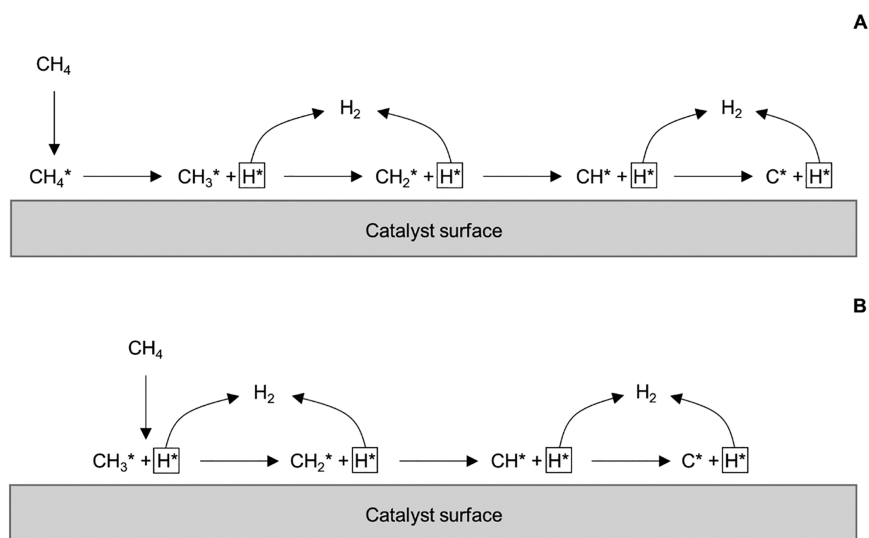
3.2. Reaction Mechanism of Catalytic Methane Pyrolysis. Several reaction mechanisms have been postulated to explain the catalytic pyrolysis reaction of methane. Some works have proposed a molecular adsorption mechanism (Scheme 3A),^{58–63} whereas a dissociative adsorption model has been described in other studies (Scheme 3B).^{64–75} In the molecular adsorption mechanism, methane is first adsorbed on the catalyst surface and then dissociates following a series of stepwise surface dehydrogenation reactions. Nevertheless, according to the dissociative adsorption model, methane dissociates upon adsorption on the catalytic active sites generating chemisorbed CH₃ and H fragments. This step is followed by the same surface dissociation reactions described

by the molecular adsorption mechanism. The dissociative adsorption mechanism emerges from studies on the interaction of methane with metal surfaces at pressures below atmospheric using molecular beam techniques with high-resolution electron energy loss spectroscopy (HREELS) and Auger electron spectroscopy.^{76–78} However, this model has also been applied to methane pyrolysis, which is usually carried out at atmospheric pressure.

Different rate-limiting steps have been proposed in the molecular adsorption mechanism. Some works consider the abstraction of the first hydrogen atom from molecularly adsorbed methane to form an adsorbed methyl group as the initiation and rate-limiting step of the decomposition of methane.^{59,63} Nevertheless, the removal of the second hydrogen from the adsorbed methyl fragment⁵⁸ or the adsorption of methane on the catalyst surface^{60,61} has also been suggested as rate-determining steps. In the dissociative adsorption mechanism, there is also no agreement on the rate-controlling step of the reaction. Some authors confirm that the dissociation of methane giving rise to a methyl group and a hydrogen atom controls the overall mechanism.^{64,75} On the other hand, according to various works on the kinetics of carbon nanotube formation, the dissociative adsorption of methane followed by the removal of hydrogen from the adsorbed methyl group limits the catalytic decomposition of methane.^{70,72,73} The kinetic models presented in the latter works differ in the number of active site types. The kinetic models for double-⁷⁰ and single-walled⁷² carbon nanotube synthesis are based on the presence of only one type of active sites, whereas that developed for the formation of multiwalled carbon nanotubes⁷³ considers two different types of active sites. Here, CH_x* and H* species are adsorbed on different kinds of active sites.

Other possible mechanisms arise from studies on the decomposition of hydrocarbons focused on the synthesis of carbon nanostructures via chemical vapor deposition. The vapor–liquid–solid (VLS) model was initially developed in 1964 to explain the crystal growth of silicon whiskers.⁷⁹ Some years later this mechanism was applied to the growth of

Scheme 3. Reaction Mechanisms Proposed for the Catalytic Methane Pyrolysis^a



^a(A) Molecular adsorption mechanism. (B) Dissociative adsorption mechanism.

filamentous carbon, which includes carbon nanotubes and nanofibers, over a nickel catalyst using acetylene as a carbon precursor.⁸⁰ The general VLS mechanism for the decomposition of hydrocarbons comprises several steps (Figure 4).^{80,81} First, the hydrocarbon is adsorbed on the catalyst

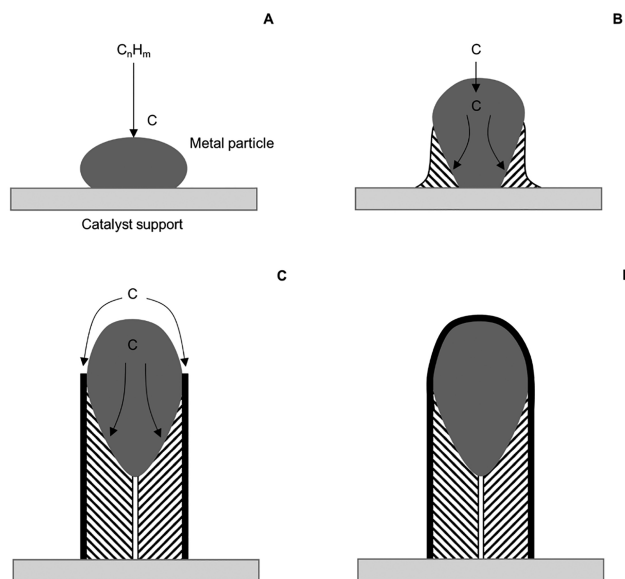


Figure 4. VLS mechanism for the growth of filamentous carbon from hydrocarbon decomposition over metal catalysts. Figure adapted with permission from refs 80 and 81. Copyright 1972 and 1989, respectively, Elsevier.

particle surface and dissociates into elemental carbon (Figure 4A). Then, carbon is taken into solution, diffuses through the bulk of the metal particle and precipitates at the backside of the catalyst particle (Figure 4B). Excess carbon accumulates at the exposed catalyst faces and is transported by surface diffusion around the catalyst particle to form the outer part of the filament. The accumulated carbon deposits force the metal particle away from the support, giving rise to the formation of the carbon filament (Figure 4C). Finally, the particle is completely encapsulated by carbon, and the filament growth ceases because there is no longer contact between the hydrocarbon and the active catalyst particle (Figure 4D).

During the third step (Figure 4C) the metal particle is distorted and elongated, and the metal is assumed to have properties of a liquid. When the metal particle is detached from the support, an initial hollow channel appears because the carbon does not have enough time to deposit in this region. The formation of filamentous carbon from the decomposition of acetylene was also studied over iron, cobalt, and chromium catalysts.⁸² The apparent activation energies for carbon growth over iron, cobalt, chromium,⁸² and nickel⁸⁰ are in agreement with those for the diffusion of carbon through the bulk of the corresponding metal. This suggests that carbon diffusion through the metal particle is the rate-determining step in the filament growth process.^{80,82} A thermal gradient may be the driving force for the bulk carbon diffusion.⁸⁰ Carbon diffuses from the hotter front face, on which the carbon precursor decomposition occurs, to the cooler backside of the catalyst particle, on which the carbon precipitates. This theory is valid when the decomposition of the carbon precursor is exothermic, as in the case of acetylene. The thermal gradient

is maintained by the exothermic decomposition of the hydrocarbon on the front face of the catalyst particle and the endothermic precipitation of the carbon at the backside. However, this hypothesis cannot explain the diffusion of carbon when the decomposition of the hydrocarbon is endothermic, as happens in methane pyrolysis. To overcome this limitation a different driving force is suggested.^{83–85} In this case, the diffusion of carbon through the metal particle derives from a carbon concentration gradient due to the different carbon solubility at the metal–gas and the metal–carbon interfaces.

Studies using high-resolution electron microscopy techniques have led to a new carbon growth mechanism.^{86,87} This mechanism does not involve the bulk diffusion of carbon species but the diffusion on the surface of the catalyst particle. The carbon species start to dissociate at the contact angle between the metal particle and the catalyst support. The accumulation of carbon at the rear part of the metal particle and the subsequent formation of lateral layers following the contour of the metal surface cause the metal particle to move away from the support, resulting in the formation of a carbon filament. The surface diffusion of carbon would also explain the hollow channel in the center of the carbon filaments.⁸⁷ Since these studies were performed with ex situ analytical methods, the microscopy images correspond to the “cold” or even deactivated catalyst. The use of in situ analytical techniques becomes thus crucial to understand the growth of carbon nanotubes and nanofibers. Images of the formation of carbon nanofibers from methane decomposition over nickel supported catalysts provided by time-resolved high-resolution in situ transmission electron microscopy demonstrate that carbon atoms do not necessarily diffuse into the bulk of the metal particles.⁸⁸ Unlike the VLS mechanism, which proposes the carbon diffusion through the metal particles as the rate-limiting stage, this model suggests that the surface transport of carbon atoms controls the rate of the nanofiber growth. This mechanism was later corroborated by other authors for the growth of nanocarbons^{89–91} and extended to the growth of graphene.⁹¹ The growth rate of carbon nanofibers over nickel, cobalt, and iron catalysts by plasma-enhanced chemical vapor deposition shows that the activation energy for carbon surface diffusion is much lower than for bulk diffusion. This would confirm the carbon diffusion on the catalyst surface as the rate-determining step for plasma-enhanced carbon growth.⁸⁹

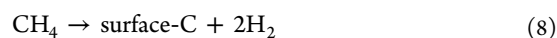
The above-described mechanisms for the growth of carbon filaments involving bulk or surface carbon diffusion correspond to a tip-growth model. In this growth model the metal particles are located at the tip of the carbon filaments since the carbon accumulated at the rear part of the catalyst particle causes its detachment from the support. The formation of carbon filaments can also follow a base-growth mechanism. Here, carbon precipitates on the apex part of the metal particle as far as possible from the support and crystallizes as a hemispherical dome. Subsequent hydrocarbon decomposition occurs on the lower surface of the particle and carbon diffuses upward, leading to the formation of carbon filaments above the metal particle, which remains attached to the support.⁹² The base-growth mechanism of carbon nanotubes is favored by strong metal–support interactions.^{93,94}

The formation of an intermediate metastable carbide phase during the nanostructure growth may also take place.⁹⁵ Here, metal particles undergo partial carburization. The metal is first transformed into a metal carbide, which is subsequently

decomposed during the synthesis of carbon filaments. The carbide cycle mechanism, that is, the decomposition of hydrocarbons through intermediate carbide-like compounds, has been reported for the growth of carbon filaments over iron and nickel catalysts.^{96–99} According to this mechanism, a metastable carbide-like intermediate compound is formed at the surface of an active catalyst particle as a result of the decomposition of the hydrocarbon. Then, the dissociation of the intermediate carbide results in the formation of carbon atoms that enter the bulk metal and lead to the supersaturation of metal by carbon. When a critical supersaturation is attained, a graphite phase is formed at the surface of the metal particle and carbon filaments start to grow. The diffusion of carbon atoms from the surface through the bulk of the metal particles to the sites of crystallization into a graphite phase takes place by a carbon concentration gradient. The decomposed intermediate carbide is restored as a consequence of the continuous dissociation of the hydrocarbon. Therefore, this cyclic process is maintained as long as there is a carbon gas source and available catalytic active sites. The presence of carbide species has been revealed for nickel catalysts in different studies.^{98,100–103} The characterization of the samples in these works was carried out using *ex situ* analytical techniques, such as transmission electron microscopy (TEM) or X-ray diffraction (XRD), after catalyst cooling. Therefore, the observed metal carbide phase could be a result of the precipitation of excess carbon on the nickel particle upon catalyst cooling.¹⁰⁴ Thus, it cannot be assured that nickel carbide is formed as an intermediate compound during the carbon growth. In addition to this, the formation of nickel carbide phases is not confirmed by *in situ* time- and depth-resolved X-ray photoelectron spectroscopy (XPS) and XRD measurements.^{105,106} This would support the fact that an intermediate carbide is not involved in the formation of carbon nanostructures over nickel catalysts.

In the case of iron catalysts, the formation of intermediate iron carbide phases has been extensively reported.^{94,100–103,107–119} Many of the works on iron catalysts were performed using *in situ* measurements.^{108,110,112,113,115,117,119} *In situ* electron microscopy images reveal that the carbide phase, which decomposes into metal and carbon, is an intermediate phase in the formation of graphite layers constituting multiwalled carbon nanotubes.¹¹⁰ Therefore, iron carbide (Fe₃C) would be involved in the growth of carbon nanotubes. The following eqs (eqs 8–11) describe the carbon nanotube growth using methane and iron catalysts.¹⁰⁰ The decomposition of metal carbides into surface graphitic carbon (eq 10) is regarded as the crucial step.

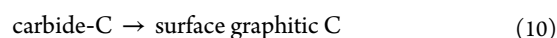
- (a) CH₄ decomposition on the catalyst surface leading to surface carbon and hydrogen:



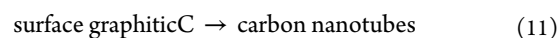
- (b) Carbon diffusion through the catalyst particles leading to carbide formation:



- (c) Formation of graphitic carbon on the catalyst surface from the metal carbide:



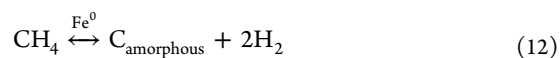
- d) Carbon nanotubes formation from surface graphite:



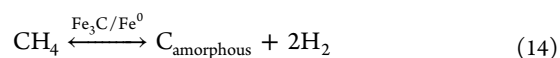
Contrary to the previous results, studies on iron and nickel catalysts based on environmental transmission electron microscopy (ETEM) and *in situ* time-resolved XPS demonstrate that a carbide phase would not be necessary for the formation of carbon nanotubes.¹²⁰ The carbide formation only occurs during the carbon nanotube growth over iron catalysts, while nickel carbide is not detected. Therefore, the growth of carbon nanotubes would not require the presence of a carbide phase.

Iron carbide may serve as an active catalyst for carbon growth^{94,113,115–117,121} and methane dissociation.^{94,118,119} A study on carbon deposition on polycrystalline iron catalysts describe different mechanisms for fresh samples and after the deposition of some carbon, as well as depending on the reaction temperature.¹²¹ Below 600 °C the rate-determining step on fresh samples is the diffusion of carbon in iron, whereas after the deposition of some carbon the rate is determined by the carbide-catalyzed hydrocarbon decomposition. Above 600 °C the surface decomposition of the hydrocarbon is assumed to be the limiting step for the carbon formation. In this case, the geometry of the catalyst surface affects the carbon formation rate on fresh samples. However, after the deposition of some carbon the rate is influenced by the iron carbide active sites instead of the geometry. The formation of γ - and α -Fe phase mixtures takes place in oxide supported iron catalysts during the reduction step prior to the chemical vapor deposition of carbon nanotubes using acetylene as a carbon source.¹¹⁷ This variation in the iron crystal structures is due to carbon contamination prior to hydrocarbon exposure. Two different growth mechanisms occur depending on the phase composition. For γ -rich iron catalyst mixtures, metallic Fe is the active phase for the growth of carbon nanotubes, whereas the formation of an iron carbide is not a prerequisite. However, for α -rich iron catalyst mixtures, the formation of Fe₃C is dominant and takes part in the carbon growth process. An investigation on nanocarbon growth over iron-based catalysts by plasma-enhanced chemical vapor deposition identifies α -Fe and Fe₃C phases depending on the growth temperature.¹¹⁶ Although at low temperatures (600 °C) only Fe₃C acts as a catalyst for the growth of carbon nanotubes both, α -Fe and Fe₃C, are active at higher temperatures. A recent study on methane pyrolysis over iron catalysts confirms that not only metallic Fe but also an iron carbide phase (Fe₃C) is active for the decomposition of methane.¹¹⁹ The proposed reaction mechanism is summarized by eqs 12–15:

- (a) Decomposition of methane on the Fe⁰ surface into amorphous carbon and hydrogen:



- (b) Reaction between the amorphous carbon and Fe⁰ to form Fe₃C or a mixture of Fe⁰ and Fe₃C, which acts as a catalyst of the reaction itself:



- (c) Diffusion of the formed carbon into Fe₃C to form supersaturated Fe₃C.

Table 2. Initial Activity of Nickel, Iron, and Cobalt Catalysts in the Decomposition of Methane for Hydrogen Production

catalyst	T [°C]	P [atm]	CH_4/N_2 [vol vol ⁻¹]	flow rate [mL min ⁻¹]	space velocity [mL h ⁻¹ g _{cat} ⁻¹]	H ₂ yield [%]	ref
Ni/CeO ₂	700	1	1/0	150	4500	53	139
Ni/La ₂ O ₃	700	1	1/0	150	4500	60	139
Ni/SiO ₂	700	1	1/0	60	7200	73	140
Fe/CeO ₂	700	1	1/0	150	4500	51	141
Fe/La ₂ O ₃	700	1	1/0	150	4500	40	141
Fe/SiO ₂	700	1	3/7	70	42000	20	94
Ni/SiO ₂	800	1	1/0	250	5000	74	134
Fe/SiO ₂	800	1	1/0	250	5000	39	134
Co/SiO ₂	800	1	1/0	250	5000	48	134

(d) Decomposition of supersaturated Fe₃C to stoichiometric Fe₃C and transformation of amorphous carbon to graphitic carbon:



From all these results, it can be concluded that different controlling steps have been proposed for the decomposition of methane. There is no general agreement, and the reaction mechanism involved in methane pyrolysis as well as the overall rate-limiting step is still unclear. Additionally, the formation of metal carbides and their role in the decomposition of hydrocarbons and nanocarbon growth is a matter of debate today. Most research on the reaction mechanism focuses on the decomposition of hydrocarbons over metal catalysts and no in-depth studies over carbon catalysts have been found. For this reason, the reaction mechanism over carbon catalysts is far from being clear. Further studies are needed to fully unravel the reaction mechanism and develop enhanced catalysts that accelerate the kinetics under optimized experimental conditions. It is essential to elucidate the reaction mechanism of methane pyrolysis and identify the determining step so that future improvements in the catalytic activity can be achieved.

4. CATALYTIC METHANE PYROLYSIS

In the absence of a catalyst the thermal decomposition of methane requires temperatures above 1000–1200 °C to achieve relevant reaction rates and methane conversions.^{6,43} Such high operating temperatures are necessary because the symmetrical molecular structure and the strong C–H bonds of methane give this molecule great stability.⁶ In order to reduce the reaction temperature and improve the hydrogen yield different metal and nonmetal catalysts (generally carbon materials) have been developed for this process over years.^{6,7,42,122} Moreover, the use of different molten metals and salts has recently attracted particular attention. Further details on the application of molten media to methane pyrolysis are described in section 6.³¹

4.1. Metal Catalysts. Transition metals, mainly nickel, iron, and cobalt, have been widely investigated as active species for methane pyrolysis. Their partially filled 3d orbitals can accept electrons from the C–H bonds of methane, which facilitates its decomposition.^{6,42,93,123–127} In addition, transition metals offer relatively high solubility and capacity for carbon diffusion through their crystalline structure.¹²⁸ Another advantage of metal catalysts is the possibility of obtaining valuable carbon nanotubes as coproduct. Nickel, iron, and cobalt are very active under moderate operating temperatures.¹²⁹ In particular, their activity exhibits the following trend: Ni > Co > Fe (Table 2).^{93,124,125,130–132} Compared to

nickel and iron, cobalt catalysts have not received much attention lately.⁶ Reasons for that are the lower activity^{133,134} and higher price than nickel, as well as toxicity problems.^{122,124,135} However, cobalt is commonly used in small amounts as a promoter of different metal-based catalysts.^{93,136–138}

4.1.1. Nickel Catalysts. Nickel catalysts show the highest initial activity among metal catalysts,^{142,143} although above 600 °C they deactivate rapidly due to carbon coking and poisoning, so that the active metal sites are encapsulated within the carbon formed during the reaction.^{6,93,124,131,136,144–148} The deactivation of the catalyst occurs when the carbon production rate, i.e., the conversion of methane, is faster than the carbon diffusion rate through the metal particles. This imbalance between the carbon production and carbon diffusion rates results in the accumulation of carbon over the metal sites, which prevents the contact of the methane molecules with the active particles and consequently deactivates the catalyst.²² To improve the stability of nickel materials, the use of suitable supports and the incorporation of different dopants have been extensively investigated.

Nickel particles are susceptible to thermal sintering in unsupported catalysts, and thus, many efforts have been made to improve their stability by the use of appropriate supports.¹³² The metal–support interaction affects the reducibility and dispersion of metal particles. Although a strong metal–support interaction hinders the reduction of nickel oxide species, it also decreases the possibility of sintering and agglomeration of nickel particles, improving their fine dispersion on the support and enabling the formation of small crystallite sizes. Consequently, the stability of the catalysts is improved.^{127,149} In some cases hardly reducible nickel solid solutions (Ni_xMg_{1-x}O)^{140,149–152} or spinel structures (NiAl₂O₄)^{153,154} are formed between the nickel particles and the support as a consequence of strong metal–support interactions. The d-orbitals of nickel in these species are completely filled and cannot accept electrons from the C–H bonds, inhibiting the adsorption and dissociation of CH₄.¹⁵³ Additionally, the difficult reducibility of nickel species prevents the formation of active metal particles.^{140,149–151,153,154} The introduction of a second oxide to the catalyst support prevents the formation of nickel structures hardly to reduce.^{153,154} For instance, the addition of TiO₂¹⁵³ or CeO₂¹⁵⁴ to the support of Ni/Al₂O₃ catalysts inhibits the formation of NiAl₂O₄ and increases the reducibility and dispersion of nickel species, which leads to improved activity and stability. Contrary to these findings, Ni/Al₂O₃·MgO shows worse catalytic performance than Ni/Al₂O₃, associated with the formation of an inactive Ni–Mg solid solution.¹⁵² Therefore, the performance of nickel catalysts is a compromise between the metal–support interaction and the

reducibility and dispersion of the metal particles. The interaction between the metal and the support has to be strong enough to avoid the aggregation of the particles and allow their fine dispersion on the support. Nevertheless, too strong metal–support interactions impede the reduction of nickel species either by increasing the reduction temperature of the nickel oxide precursors or by the formation of hardly reducible species between the metal and the support that prevent the formation of active metallic nickel.¹⁵⁵ In addition to this, a strong metal–support interaction can inhibit carbon diffusion, leading to a faster catalyst deactivation.¹⁵⁶ Therefore, a suitable metal–support interaction has to result in well-dispersed and easily reducible nickel particles and, at the same time, allow an appropriate carbon diffusion through them.

The role of promoters in metal catalysts is to create a balance between the rates of methane dissociation and carbon diffusion, that is, to modulate the dissociation rate of methane and increase that of carbon diffusion.¹⁵⁷ The addition of a second metal as a promoter, such as palladium or copper, allows working at higher temperatures without rapid catalyst deactivation. Since the decomposition of methane is an endothermic reaction, the possibility of operating at higher temperatures results in better methane conversions and hydrogen yields.^{128,158} Palladium and especially copper are the most common promoters of nickel catalysts. These metals are not active for methane dissociation because of their filled 3d orbitals, but they can significantly affect the electronic properties of nickel.^{157,159–161} Ni–Cu and Ni–Pd catalysts deactivate above 700 °C, although their stability and the deactivation temperature can be increased with increasing the promoter loading.^{125,158,162} The good stability of promoted catalysts is due to the formation of metal alloys with high lattice constants, which are able to accumulate larger carbon amounts without deactivation.^{128,158} Additionally, the higher carbon diffusion rate through the corresponding alloys rather than through the pure nickel particles prevents the formation of encapsulating carbon on the active sites.^{125,128,156,158} As a result, the generation of filamentous carbon is favored over the formation of encapsulating carbon, which consequently extends the catalyst lifetime.¹²⁵ In addition to this, promoters improve the fine dispersion of nickel particles on the catalyst support^{131,163–166} and the reducibility of nickel oxide species. The better reducibility is associated to the hydrogen spillover effect induced by the promoter. Copper and palladium are active sites for the dissociation of hydrogen molecules, and thus, facilitate the conversion of nickel oxide species into metallic nickel during the reduction step prior to the reaction.^{127,128,165–167} The presence of a larger number of weakly interacted nickel species on the support after doping may also benefit the reducibility^{156,158,165,166} and prevent the formation of hardly reducible nickel structures.^{131,163}

The dopant loading in nickel catalysts is a crucial parameter. Catalysts with higher promoter loadings are stable at higher temperatures, and thus, the deactivation temperature grows with the content of the dopant.^{125,158,162} The higher lattice constants of highly doped catalysts might explain this fact.^{158,162,168} Nevertheless, there is an optimized promoter loading for a given reaction temperature.^{125,131,145,146,162,167} The addition of small dopant amounts results in stable materials with a good metal dispersion and small crystallites that inhibit nickel sintering.¹⁴⁶ However, excessive promoter loadings lead to faster deactivation and worse thermal stability of the catalyst due to the dramatic decrease in surface area and

the formation of large, poorly dispersed nickel crystals.^{125,146,167}

4.1.2. Iron Catalysts. Although iron is less active than nickel for the decomposition of methane, iron catalysts are more resistant to carbon coking and poisoning at high temperatures.^{136,144,169} At low reaction temperatures (<600 °C) nickel-based catalysts exhibit superior catalytic performance, whereas iron materials are still active at higher temperatures at which nickel catalysts deactivate very fast. Unlike nickel, iron materials are stable up to 700–1000 °C.^{6,119,144,170} The higher stability is related to the carbon diffusion rate, which is 3 orders of magnitude higher through iron compared to nickel.^{130,131,149} Thus, iron catalysts keep a better balance between the rates of carbon production and diffusion, leading to a longer catalyst lifetime. Compared to cobalt- and nickel-based materials, iron catalysts are inexpensive and non-toxic.^{119,171–175} Furthermore, the carbon coproduct in iron-catalyzed reactions is free of harmful metals and thus has the potential to be traded or safely stored. For these reasons, iron catalysts are the preferred option to industrialize the pyrolysis process of methane.^{174,176}

Metal promoters influence different catalyst properties (reducibility, surface area, metal dispersion, carbon capacity) and lead to the formation of bimetallic materials that are catalytically more active and stable compared to the corresponding monometallic iron catalysts. An adequate promoter enhances the reducibility of iron oxide species into metallic iron by decreasing the reduction temperature, probably due to the hydrogen spillover effect created by the promoter. A better reducibility of iron catalysts is observed after the addition of cobalt, copper, palladium, molybdenum, and nickel.^{136,177–180} Another advantage of catalyst doping is the increase in the surface area, which takes place over Fe–Mo^{179,181,182} and Fe–Co^{123,182} catalysts. Furthermore, the greater metal dispersion in different bimetallic materials (Fe–Co, Fe–Ni) affects positively the catalytic performance.¹³⁷ The incorporation of a second metal (Ni, Co) also leads to higher carbon capacities and decreases the carbon deposition rate over the active sites due to the balance between the carbon atom formation, diffusion, and precipitation. Consequently, the promoted iron catalysts are more stable and exhibit longer catalyst lifetimes.^{123,136,147,183}

Supported and unsupported iron catalysts as well as different iron organometallic precursors have been investigated in the decomposition reaction of methane. Unsupported and highly iron-loaded materials have a low catalytic activity and deactivate quickly due to the small iron surface area.¹⁸⁴ Bulk iron catalysts are highly susceptible to deactivation also because of their large particle size.¹⁷⁰ Additionally, the poor dispersion of metal particles and the formation of a solid solution between the metal and the support are responsible for the low methane conversion over highly metal-loaded catalysts.¹⁸⁴ Thus, the support plays a crucial role in the suitable dispersion of the iron particles and the maintenance of an effective metal surface during the reaction.¹⁸⁴ The incorporation of a support reduces the sintering effect, so that supported catalysts present a remarkably higher stability.¹⁷⁰ For these reasons, iron catalysts prepared on a suitable support are preferred over unsupported materials. Al₂O₃ is the most common support of iron catalysts. The combination of Fe⁰ and Al₂O₃ keeps a balance between the rate of methane decomposition, and thus, the carbon formation, and the diffusion rate of carbon through the

catalyst particles, avoiding the fast formation of encapsulating carbon.¹¹⁹ The formation of some spinel structures (FeAl₂O₄, MgFe₂O₄, Fe₂SiO₄) between the metal and the support may also take place.^{119,126,147,149,174,177,181} Nevertheless, their role in the catalytic activity is still unclear. FeAl₂O₄ species are detected in some Fe/Al₂O₃ catalysts. Although FeAl₂O₄ is inactive for methane decomposition, the interaction between the metallic iron particles and FeAl₂O₄ may play a positive role as the FeAl₂O₄ species can enhance the catalytic activity by preventing the agglomeration of metal particles through the strong bonding between Fe and FeAl₂O₄.^{119,174,177} Different iron species are found in several Fe/Al₂O₃ catalysts depending on the reduction temperature. Here, the samples with a combination of Fe⁰ and FeAl₂O₄ are more active than those containing Fe⁰ and Fe₃O₄.^{119,174} The formation of FeAl₂O₄ spinel structures is not observed in other works, but the strong interaction between iron and the alumina support is also beneficial because it prevents metal particles from agglomeration.⁹⁴ Contrary to these results, the strong metal–support interaction and the spinel formation are reported to be unfavorable.¹⁴⁷ Different iron species, and hence, different catalytic activities may be observed depending on the catalyst preparation method. For example, Fe/Al₂O₃ catalysts synthesized by impregnation are more active and stable than those prepared by coprecipitation. Catalysts synthesized by coprecipitation contain Fe₂O₃ and Fe species, whereas the catalysts prepared by impregnation present spinel species (FeAl₂O₄) and Fe₃O₄ in addition to some Fe₂O₃ and Fe species.¹²⁶ The activity is related to the presence of Fe²⁺ in FeAl₂O₄ and Fe₃O₄ phases but not to the formation of a spinel structure itself, as stated in other works.^{119,174,177} The appearance of Fe²⁺ in the samples synthesized by impregnation may be positive for the formation of catalytic active sites via in situ reduction during methane decomposition. The impregnation method may also be suitable due to the low interaction between iron and Al₂O₃ and the easier reduction of the resulting catalysts.¹⁴⁷ The appearance of the MgFe₂O₄ spinel phase is detected in some Fe/MgO catalysts as well.^{149,181} The existence of MgFe₂O₄ indicates a strong metal–support interaction, which hinders the reduction of the iron oxide precursor.¹⁸¹ The low surface area of the catalyst and the difficult reduction of the metal particles may be the reasons for the poor activity of Fe/MgO.

Different organometallic compounds, such as iron pentacarbonyl (Fe(CO)₅) and ferrocene (iron dicyclopentadienyl, Fe(C₅H₅)₂), have mainly been intended for the production of carbon nanotubes. Fe(CO)₅ decomposes at temperatures higher than 300 °C (eq 16),⁷¹ whereas the decomposition of ferrocene takes place above 500 °C (eq 17):^{71,185}



Ferrocene has been more widely used than Fe(CO)₅. This is probably due to the low cost, innocuousness, and nontoxicity of ferrocene in contrast to Fe(CO)₅.¹⁸⁵ Ferrocene is a suitable organometallic compound for carbon nanotube growth since it not only gives rise to small iron metal particles but also acts as a carbon source upon its thermal decomposition. The formed iron particles agglomerate into clusters that serve as a catalyst for the decomposition of the reactive carbon species produced in the gas phase (eq 17). The carbon resulting from these species constitutes the source for the subsequent formation of carbon nanotubes that nucleate and grow on the iron clusters.

A hydrocarbon is often injected as an additional carbon source. The hydrocarbon decomposes on the iron particles and produces extra carbon for the formation of larger nanotube amounts.¹⁸⁶ The experimental setup for this process usually consists of a low and a high temperature furnace.^{72,73,187–190} Ferrocene sublimes in the first oven at low temperature (>150 °C). Then, ferrocene as a vapor is carried by a gas stream (Ar, H₂, N₂ and/or hydrocarbons such as acetylene, methane, benzene) into the second furnace at a higher temperature (800–1100 °C). In the second oven ferrocene and the additional hydrocarbon decompose, giving rise to the growth of carbon nanotubes. Ferrocene and Fe(CO)₅ have also been employed as iron catalyst precursors for the pyrolysis of methane with the aim of producing hydrogen, although this application has been rarely reported.⁷¹ In this case, the iron clusters derived from the decomposition of the organometallic compound act as an in situ generated catalyst. Since different gaseous products result from the breakdown of Fe(CO)₅ (eq 16) and ferrocene (eq 17), the outlet gas must be cleaned to remove the undesirable impurities (CO, C₃H₆) and obtain high quality hydrogen. The poisoning of the outlet gas with unwanted compounds may explain the scarce application of these organometallic catalyst precursors in the decomposition of methane for hydrogen production.

4.1.3. Regeneration of Metal Catalysts. Different regeneration methods can be employed to remove the carbon deposits from metal catalysts and restore their activity. The reactivation techniques include combustion with oxygen or air of the carbon byproduct^{191–197} and gasification with steam^{191,195,198,199} or carbon dioxide.^{195,196,200} During oxygen/air regeneration the carbon deposits are burned with oxygen, giving rise to CO₂ in a complete combustion and CO if the oxidation is incomplete. This technique has been used to restore the activity of nickel catalysts. All the carbon on the catalyst surface is eliminated after combustion in air at 550–600 °C.^{191,192,195} The initial activity for hydrogen production is restored after regeneration^{192,193,195} but the deactivation rate of the regenerated catalyst is much faster compared to the fresh catalyst.^{192,194,197} This fact is attributed to the increase in the crystallite size due to particle sintering,¹⁹² the disintegration of the catalyst into fine powder, and the change in the face planes of the metal atoms occurring during the regeneration.¹⁹⁴ The disintegration of the catalyst may also be related to the destruction of the porous support during the filament growth.¹⁹⁴ The combustion of carbon involves an exothermic reaction so that the release of heat can give rise to high temperatures in the reactor and harm the catalyst.¹⁹⁴ To avoid damaging the catalyst the regeneration with air should be accomplished in a fluidized-bed reactor since in a fixed-bed reactor some hot spots may be formed.¹⁹⁵ Using a low oxygen concentration can also help to avoid high temperatures in the reactor.¹⁹⁷ The heat released during the oxidation of the carbon can be used to thermally sustain the endothermic reaction of methane decomposition.^{193,195} The regeneration with air is much faster than with steam or CO₂,^{195,196} but unlike these techniques, the initial metallic nickel is converted to nickel oxide during air combustion and the catalyst has to be reduced again before the next reaction cycle.^{191,192,195,196} In the gasification process with steam, carbon reacts with water steam, and a gaseous mixture composed of CO_x and H₂ is obtained. One advantage of this procedure is the avoidance of a new reduction step because the metallic nickel form is preserved.^{191,195} Furthermore, additional hydrogen can be

Table 3. Determining Factors of the Activity and Stability of Carbon Catalysts

determining factors of activity	ref	determining factors of stability	ref
defect concentration	68,69,144,201,203–206,210–215	total surface area	217,218
surface area	68,69,204,211–213,215	external surface area	69,129,207,209,212
concentration of surface oxygenated groups released as CO and CO ₂	206,217,218	pore volume	201,208,213,221
concentration of surface oxygenated groups desorbed as CO	208	structure (interconnected mesoporosity)	69,129,207,209

produced by steam gasification, which leads to higher global hydrogen yields.^{191,198} However, the regeneration with steam requires long times and not all carbon species can be removed.¹⁹⁵ Although a small amount of carbon deposits is not eliminated with steam, neither structural changes in the nickel particles nor a significant loss of catalytic activity occur after several successive decomposition–regeneration cycles.¹⁹⁸ The reactivation process by CO₂ gasification results in the formation of CO. This method preserves the reduced state of the metal^{195,196} but also requires long regeneration times.¹⁹⁵ The application of CO₂ regeneration is limited by the low carbon removal rate and the high endothermicity of the reaction.¹⁹⁶

All the regeneration methods described above lead to the formation of CO_x products, which is an important drawback taking into account the clean nature of methane pyrolysis. In addition to this, the carbon byproduct is destroyed, and the carbon nanotubes cannot be recovered. An additional technique to overcome these problems is catalyst regeneration by using an acid or a base.⁹⁴ This procedure enables not only the separation, purification, and generation of highly pure and crystalline carbon products, but also the reactivation of metal catalysts. The formation of base-grown instead of tip-grown carbon nanotubes is required to avoid catalyst damage. If the metal particles were located at the tip of the carbon nanotubes, they would be dissolved in the acid or base and the catalyst would be destroyed. Contrary to tip-grown carbon nanotubes, base-grown carbon nanotubes, where the metal particles remain attached to the support, can be easily harvested without sacrificing the catalyst. Nevertheless, the use of homogeneous acids to remove the carbon deposits is contraindicated at the industrial level and should be avoided.

The regeneration of the spent catalyst may improve the economics of the process, but constitutes a real challenge for scaling-up. The reactivation technique should be energy efficient and environmentally friendly, with short regeneration times, and generate a catalyst with good catalytic performance. Nevertheless, none of the state-of-the-art methods meet these requirements²² and more in-depth studies are essential to advance the development of the pyrolysis process on a large-scale.

4.2. Carbon Catalysts. Carbon materials are usually less active than metal catalysts and require higher reaction temperatures, normally between 800 and 1000 °C, depending on the type of carbon.^{6,9,176} However, carbon catalysts are more stable and exhibit longer catalyst lifetimes. The application of carbon materials in methane pyrolysis has been widely investigated in recent years due to their significant advantages over metal catalysts for the industrialization of the process. Compared to metal catalysts, carbon materials are significantly cheaper. In addition, the resulting carbon product may also have catalytic effects so that the decomposition of methane could be sustained for longer times without an important activity decay. In this case, the carbon catalyst would

be required only for the initiation of the reaction, and the separation of the carbon product from the carbon catalyst may not be essential. Consequently, CO₂ emissions resulting from the regeneration process could be prevented. Carbons are also resistant to sulfur and other impurities contained in natural gas, and hence, it would not be necessary to purify the feed gas before entering the reactor. The nontoxicity of the resulting carbon after reaction and the possibility of its subsequent use or secure storage are additional determining factors for the industrial implementation of methane pyrolysis based on carbon catalysts.

Activated carbons and carbon blacks are the most common carbon materials, but some others, such as graphite, diamond powder, carbon nanotubes, glassy carbon, fullerene soot, fullerenes C_{60/70}, acetylene black, coal char and ordered mesoporous carbons (CMK materials), have also been investigated.⁶⁸ Amorphous carbons (activated carbon, carbon black, acetylene black, coal char) have a disordered structure with a large number of high-energy sites (HES) on their surface. HES include dislocations, low-coordination sites, vacancies, atoms with free valences, discontinuities, edges, defects, and other energetic abnormalities. It is generally accepted that HES constitute the main fraction of active sites in carbon catalysts so that the number of HES determines their catalytic activity. For this reason, amorphous carbons, which have a high defect concentration, are usually more active than well-ordered materials. The carbon atoms in HES react with methane molecules in order to compensate their charge and stabilize themselves energetically, giving rise to the decomposition of methane.

Among the amorphous structures, activated carbons and carbon blacks are the most used materials due to their high activity.^{6,7,9,33,201} Although activated carbons are initially more active than carbon blacks, carbon blacks are more stable and show longer catalyst lifetimes.^{68,69,144,202–211} Different catalyst properties determine the activity and stability of carbon materials, as shown in Table 3.

4.2.1. Activity of Carbon Catalysts. The threshold temperature, which defines the temperature at which hydrogen starts to be produced, has been used as a measure of the initial activity of carbon catalysts.^{69,144,207,209,212} Low threshold temperatures are equivalent to high catalytic activities. Activated carbons (mesoporous and microporous), carbon blacks (black pearls 2000 and Vulcan XC72) and CMK catalysts (CMK-3 and CMK-5) exhibit the lowest threshold temperatures, and hence, the highest initial activity. Their high initial activity is linked to the large density of graphene defects, which are preferential sites for methane adsorption and dissociation. A direct linear relationship exists between the amount of defects on the graphene layers and the threshold temperature^{69,144} as well as the initial reaction rate.²¹³ This fact strongly supports that the surface defects are the main active sites of carbon catalysts. Additionally, the defect concentration and the degree of order, that is, the crystallinity of the carbons,

are correlated parameters. Disordered structures, such as activated carbons and carbon blacks, usually have a high defect concentration and low crystallinity.^{68,129,144,206,209,214} However, CMK materials present a special behavior since, despite having a high density of carbon defects, they show an intermediate crystallinity.⁶⁹ The initial activity has not only been related to the threshold temperature but also to the initial methane decomposition rate at constant temperature. Despite this difference in the measure of initial activity, there is general agreement that carbons with a greater number of surface defects are catalytically more active.^{68,201,203–206,210,211,213–215}

Although the defect concentration of the carbon structure seems to be the most important parameter affecting the catalytic activity, other factors, such as the specific surface area and the concentration of oxygenated groups, can also influence the catalyst performance. For instance, carbons with higher surface areas usually exhibit superior catalytic activities than poor surface area materials.^{68,204,215} An approximately linear relationship in logarithmic scale has been established between the initial activity of different carbon samples and their surface areas. In other cases, despite the greater catalytic activity of carbons with larger surface areas, the relationship between both parameters is not linear.^{69,211–213} Hence, the surface area cannot be the only determining factor, and the number of defects also plays a crucial role. The increase in surface area results in an increment of the number of active sites (defect concentration).^{68,69,205} However, the catalytic activity correlates quantitatively better with the defect concentration in the graphene layers rather than with the surface area.⁶⁹ Contrary to these results, different activated carbons exhibit similar initial activities regardless of the surface area. This suggests that only a part of the surface area is involved in the decomposition of methane.²¹⁴ In other studies, carbons with comparable surface areas show very different catalytic activities, which also indicates an apparent nonrelationship between the surface area and the activity.^{68,204,215} This was observed when comparing carbons of a different nature. For instance, activated carbon from hardwood displays a higher activity than carbon black (black pearls 2000) despite their similar surface areas. The same tendency was detected with structurally close carbons with the same surface area, such as carbon black and acetylene black.^{68,204,215} The higher activity of carbon black is attributed in this case to the larger amount of oxygenated surface groups. Different trends were observed when analyzing the activity of several coal chars and activated carbons.²¹⁶ When only coal chars are compared, an increase in the surface area leads to an increase in the initial activity for methane decomposition, although the relation is not linear. However, coal chars and activated carbons with very different specific surface areas can show similar activities. Here, the nature of the carbon plays a decisive role.

The concentration of oxygenated groups on the surface of carbon catalysts may also have an effect on the initial activity. Two different mechanisms explain their influence. Oxygenated groups can react directly with methane, or can be released as CO and/or CO₂, which are active reaction sites for methane decomposition.²¹⁷ An approximately linear correlation between the initial methane conversion rate and the concentration of oxygenated groups desorbed as CO and CO₂ has been reported.^{206,217,218} Also, a good correlation has been established between the initial reaction rate and the concentration of oxygenated groups desorbed only as CO, whereas those groups released as CO₂ do not show any

influence.²⁰⁸ The exponential decay of the reaction rate during the initial period of the reaction may be due to the decrease of the surface oxygenated groups²¹⁹ but also to the partial coverage of defects (active sites) by the carbon formed during the first stages of methane decomposition.¹²⁹ Most of the oxygenated groups should be removed during the heating process before the reaction begins,¹²⁹ so that the initial activity cannot be attributed exclusively to them.^{69,129} Although oxygen groups may have an impact on the initial activity, surface defects constitute the main part of active sites.⁶⁸

4.2.2. Stability and Deactivation of Carbon Catalysts.

Although carbon materials usually display longer catalyst lifetimes and higher resistance to carbon coking and poisoning than metal catalysts, they also become gradually deactivated. The long-term efficiency and stability of carbon catalysts are often evaluated from their capacity for carbon accumulation before deactivation.²¹⁷ Catalysts able to accumulate larger carbon amounts provide a more stable and sustained hydrogen production for longer times. The stability of carbon catalysts may be determined by a combination of pore size distribution and specific surface area. Mesoporous carbons with high surface areas often lead to a more sustainable hydrogen production because of their larger capacities for carbon deposition. On the contrary, the catalytic activity over microporous carbons decays more rapidly due to the lower carbon capacity and the greater mass transport limitations occurring in micropores. Even if the pores are not completely filled with carbon deposits, the narrowing of the pore mouth can also prevent the diffusion of methane molecules into the pores leading to the decrease of the catalytic activity.^{68,201} Additionally, a more or less linear relationship exists between the surface area of the fresh catalyst and the stability, that is, catalysts with higher surface areas can accommodate higher carbon amounts before deactivation, and thus, provide long-term efficiency and sustainability.^{217,218} According to the evolution of the conversion of methane and the surface area over time, which show the same trend (initial drop followed by shallow decline),⁶⁸ the catalyst deactivation may occur as a consequence of the loss in surface area.^{68,201,202,217} Contrary to these results, no relationship was found between the surface area and the long-term sustainability in other works. Therefore, catalysts with similar surface areas would not necessarily accumulate the same amount of carbon deposits.^{206,213} In this case, the pore size distribution plays a decisive role.²¹³ Carbon catalysts may also lose their activity by the progressive filling and blockage of the pores.^{144,209,217,220} For this reason, the pore volume is an important parameter that affects the catalyst lifetime since a bigger pore volume offers a larger space to accommodate carbon deposits.^{201,208,213,221} The pore volume defines the maximum amount of carbon deposits before deactivation and determines the maximum hydrogen production per mass of catalyst.²²¹ There is actually a linear correlation between the catalyst pore volume and the mass of carbon accumulated until deactivation²⁰⁸ as well as the total hydrogen production.²¹³ Furthermore, the deactivation of carbon catalysts may be partly explained by the loss of oxygenated groups on the surface over reaction time.²²¹ Before catalyst deactivation the carbon product derived from methane decomposition may also have some catalytic effects. This fact is revealed by several kinetic studies, in which the carbon deposition rates are calculated throughout the reaction.^{129,208,219} Three different zones are identified along the reaction rate curves from the start of the reaction to catalyst

deactivation. The first zone corresponds to an exponential decay of the catalytic activity, attributed to the removal of oxygenated groups from the catalyst surface,^{208,219} or to the partial coverage of defect sites by the carbon product.¹²⁹ The second zone is characterized by an increase in the reaction rate. This fact denotes an autocatalytic effect, which indicates that the carbon produced from methane is also catalytically active. Nevertheless, the activity of these new active sites is clearly lower than the active sites in the fresh sample. In the last part of the kinetic curve, the reaction rate decreases until the catalyst completely deactivates. This zone may correspond to the deactivation of the new active sites¹²⁹ or the drop in the effective surface area and pore volume.^{208,219}

CMK materials, which are ordered mesoporous catalysts, and carbon blacks show the highest stability among carbon catalysts. Carbon blacks have well-defined concentric graphene layers that generate large interparticle spaces.¹⁴⁴ In addition to this, although some carbon blacks have a significant contribution of micropores to the overall surface area, they possess a high external surface area.^{207,209,212} Depending on the catalyst nature and pore structure, the carbon product remains within the pores, causing their blockage and leading to catalyst deactivation, or leaves the pores and grows to the outer part of the catalyst particles.⁶⁹ The latter mechanism is expected to occur in catalysts with a high proportion of external surface area (carbon blacks)^{69,129,207,209,212} or an ordered and interconnected mesoporosity (CMKs).^{69,129,207,209} The ability of carbon deposits to move and grow toward the outside part of the particles avoids pore blockage and improves the accessibility of methane molecules even after the deposition of significant amounts of carbon. All this explains the higher resistance of CMK materials and carbon blacks to carbon deactivation. Activated carbons have been widely investigated for methane pyrolysis due to their high initial activity. However, they show a poor long-term stability. Microporous activated carbons are quickly deactivated due to the micropore blockage caused by carbon deposits.^{69,207,209,212} Mesoporous activated carbons exhibit longer lifetimes than microporous materials, but the activity decay is relatively faster in comparison to carbon blacks.^{144,209} The reasons for the low stability of mesoporous activated carbons despite the high contribution of mesopores and the high share of external surface area remain unclear.

4.2.3. Regeneration of Carbon Catalysts. Different regeneration methods can restore the original activity of carbon catalysts. The regeneration techniques include combustion with oxygen or air²²² and gasification with CO₂^{218,223,224} or steam.^{225,226} The activity of carbon catalysts can be partially recovered by burning the carbon deposits with highly diluted oxygen in nitrogen. Nevertheless, the catalyst itself can also react with oxygen because it is usually more reactive than the carbon byproduct, resulting in the loss of a part of the original catalyst.²²² Via a CO₂ gasification regeneration process, the initial catalytic activity and the carbon accumulation decrease after each reactivation cycle.^{218,224} The reduction of the surface area and the concentration of surface oxygenated groups occur after each reaction–CO₂ regeneration cycle.²¹⁸ This may be due to the removal of a part of the initial catalyst, which is less resistant to CO₂ gasification than the carbon deposits. In fact, after several reaction–regeneration cycles the carbon catalyst consists mainly of carbon derived from the reaction itself, whereas the initial catalyst has been gasified. The decrease of surface

oxygenated groups would reduce the initial methane decomposition rate, and the lower surface area would decrease the capacity for carbon accumulation and shorten the catalyst lifetime. Concerning the steam gasification process, this method significantly increases the surface area of the deactivated carbon catalyst, which allows almost complete restoration of the original activity.^{225,226} Even after several reaction–regeneration cycles the initial activity is completely recovered by means of the steam activation procedure.²²⁵ In this case, the disordered and highly reactive pyrolytic carbon deposits obtained during methane decomposition are more easily oxidized than the catalyst itself.²²⁶ Therefore, steam gasification seems to be the most suitable regeneration technique to recover the initial catalytic activity of carbon catalysts. Furthermore, additional hydrogen is produced during the reactivation with steam, and thus, the overall hydrogen yield is enhanced.⁶ The activity of carbon catalysts is partially or completely recovered by the previous regeneration procedures. Nevertheless, CO_x emissions are generated in all cases. Therefore, the commercialization or storage of the resulting mixture of catalyst and carbon coproduct are the most suitable options to prevent any CO₂ emissions. Unlike nickel and cobalt catalysts, carbon materials are cheaper and nontoxic, which are important advantages over these metal catalysts to industrialize the process.

4.2.4. Co-feeding as a Way to Extend the Lifetime of Carbon Catalysts. Co-feeding of methane with minor amounts of other hydrocarbons can improve the catalytic activity of carbon materials and partially overcome deactivation problems. The addition of a second compound to the methane feed gas aims to generate a catalytically active carbon product to keep a good activity for longer times.^{68,202,227–232} Methane has been co-fed with saturated (propane), aromatic (benzene), and unsaturated (acetylene, ethylene) hydrocarbons.^{68,202} An accelerating effect on the decomposition rate of methane takes place when aromatic and unsaturated hydrocarbons are introduced. Moreover, a steady-state hydrogen production is achieved. Carbons produced from ethylene and especially from acetylene and benzene are catalytically more active for the decomposition of methane than the carbon derived from methane itself. There is a good correlation between the activity and the crystallite size of the carbon product. The smaller crystallites produced from benzene, acetylene, and ethylene possess a higher surface concentration of HES and consequently lead to greater catalytic activities. Nevertheless, carbon deposits from propane display a similar activity to that of methane-derived carbon and its incorporation does not result in a significant stability improvement.⁶⁸ This may be due to the comparable size and structure of the carbon products derived from the same family of saturated hydrocarbons (methane and propane).²⁰² In contrast, a beneficial effect of adding alkanes, such as ethane, has been observed in the noncatalytic methane pyrolysis.²³³ Here, the activation of methane and the subsequent formation of methyl radicals occur by the attack of radical species generated from the pyrolysis of ethane. These methyl radicals are successively incorporated into the pyrolysis products via radical reactions. Thus, methane can be activated by radicals generated from coexisting molecules without the use of a catalyst or operation at extremely high temperatures. The incorporation of an inert gas causes an analogous effect.⁵⁶ In this case, the activation of methane molecules occurs upon collision with the molecules of the inert gas, which accelerates the overall reaction. The co-

feeding with propylene,²²⁸ ethylene,^{227,229} and ethanol²³¹ can also reduce the deactivation of carbon catalysts and stabilize the catalytic activity for longer times. CO₂ as a co-fed gas allows the partial regeneration of the deactivated catalyst by *in situ* carbon gasification. Although CO₂ leads to the stabilization of carbon catalysts, its incorporation is not favorable from the energetic and environmental point of view.²³⁰

The co-feeding of methane is questionable for the industrialization of the process. The viability may be determined by the cost and the required amount of the co-fed compounds.⁶ Depending on the final hydrogen application, the feasibility of the industrial implementation may be conditioned if additional purification steps are necessary to remove the unconverted co-fed compounds from the final gaseous product.⁹ Therefore, further research is needed to elucidate whether the addition of a second compound to the methane feed gas is worthwhile on an industrial level.

5. OPERATING CONDITIONS

The decomposition of methane involves an endothermic reaction, and hence, the conversion of methane and the production of hydrogen are favored by high temperatures (Figure 5).^{7,9} However, an increase in methane conversion also

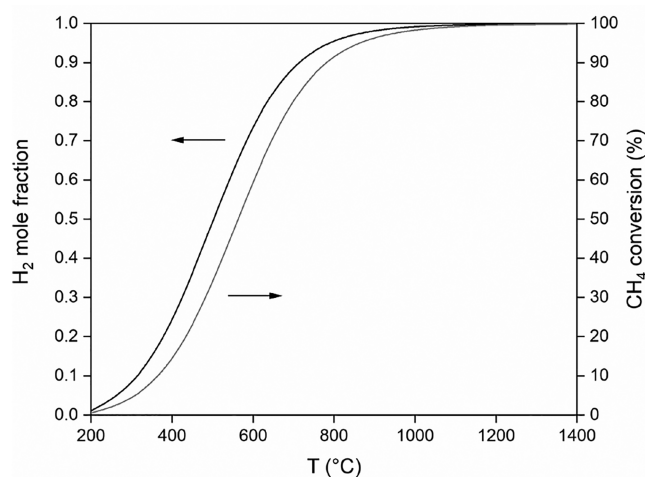


Figure 5. Hydrogen mole fraction (in the gas phase excluding carbon) and methane conversion in the thermodynamic equilibrium of methane pyrolysis at 1 bar and different temperatures (calculated using Aspen Plus software).

leads to a higher carbon production rate. In the catalytic decomposition of methane, this results in an imbalance between the carbon production and the carbon migration rates through the catalyst particles, which consequently accelerates the deactivation of the catalyst.^{125,130} Any factor that increases the rate of methane decomposition without an equivalent improvement in the rate of carbon transfer promotes the rapid loss of catalytic activity.¹³⁰ In the case of metal catalysts, the particles can sinter at high temperatures, which also favors the catalyst deactivation.^{124,127,162,167,174,234–241}

Carbon materials are less active than metal catalysts and require higher operating temperatures, usually between 800 and 1000 °C (Figure 6). There are also differences in the optimum operating temperature range depending on the type of metal catalyst. Nickel catalysts are more active but

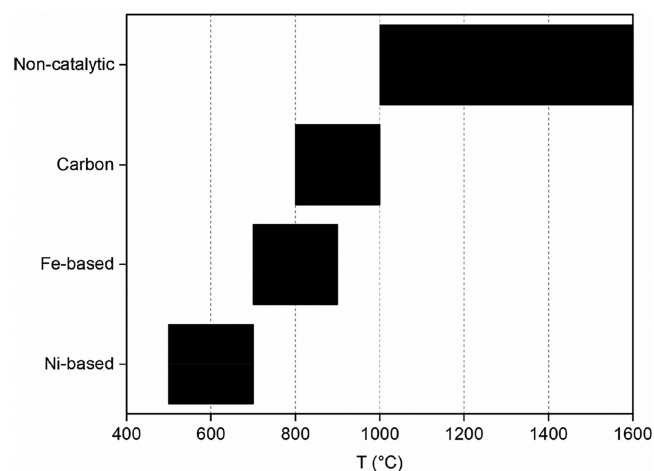


Figure 6. Temperature range of applicability of different catalysts for methane pyrolysis according to ref 22.

deactivate more rapidly than iron catalysts at high temperatures. For this reason, experiments over nickel materials are carried out in a lower temperature range (500–700 °C) than iron catalysts (700–900 °C) (Figure 6).²²

According to Le Chatelier's Principle, lower reaction pressures shift the equilibrium toward the formation of hydrogen, giving rise to a gas product with a higher hydrogen mole concentration (Figure 7A). Since keeping pressures lower than atmospheric is costly and complex, an inert gas, such as nitrogen or argon, is usually incorporated to the feed gas (Figure 7B). The addition of an inert gas decreases the partial pressure of methane, while the total pressure is maintained at 1 bar.¹⁰ At constant temperature and for the same amount of catalyst, the mass of carbon deposited per mass of catalyst decreases with a reduction in the partial pressure of methane due to a dilution effect.^{242–244} Therefore, the incorporation of an inert gas has a positive effect on hydrogen production and catalyst stability. Nevertheless, the main disadvantage is the requirement of additional separation and purification processes,¹⁰ and thus, dilution with an inert gas may not be feasible for the industrialization of methane pyrolysis.

High gas hourly space velocities (GHSVs) lead to short residence times and low contact efficiencies between the gas molecules and the catalyst. As a consequence, the amount of methane adsorbed on the catalytic active sites as well as methane conversion rate decreases.^{125,130,131,164,167,245–248} High GHSVs also cause an imbalance between the rates of carbon formation and diffusion through the catalyst particles, which favors the carbon accumulation²⁴⁹ and accelerates the catalyst deactivation.^{167,181,247} For instance, in a fluidized-bed reactor an increase in GHSV promotes the mixing between methane and the catalyst particles due to the better gas–solid contact. Nevertheless, excessive values give rise to the formation of more and bigger bubbles, which affects negatively the interaction between the reactants and the catalyst. Therefore, a compromise between a good mixing and the formation of bubbles must be found.²³⁵

Despite the numerous investigations on the effect of different operating conditions, they all focus on research at the academic level. As there are no industrially developed processes, the operating conditions are still unknown for industrial application. Further studies are required to find

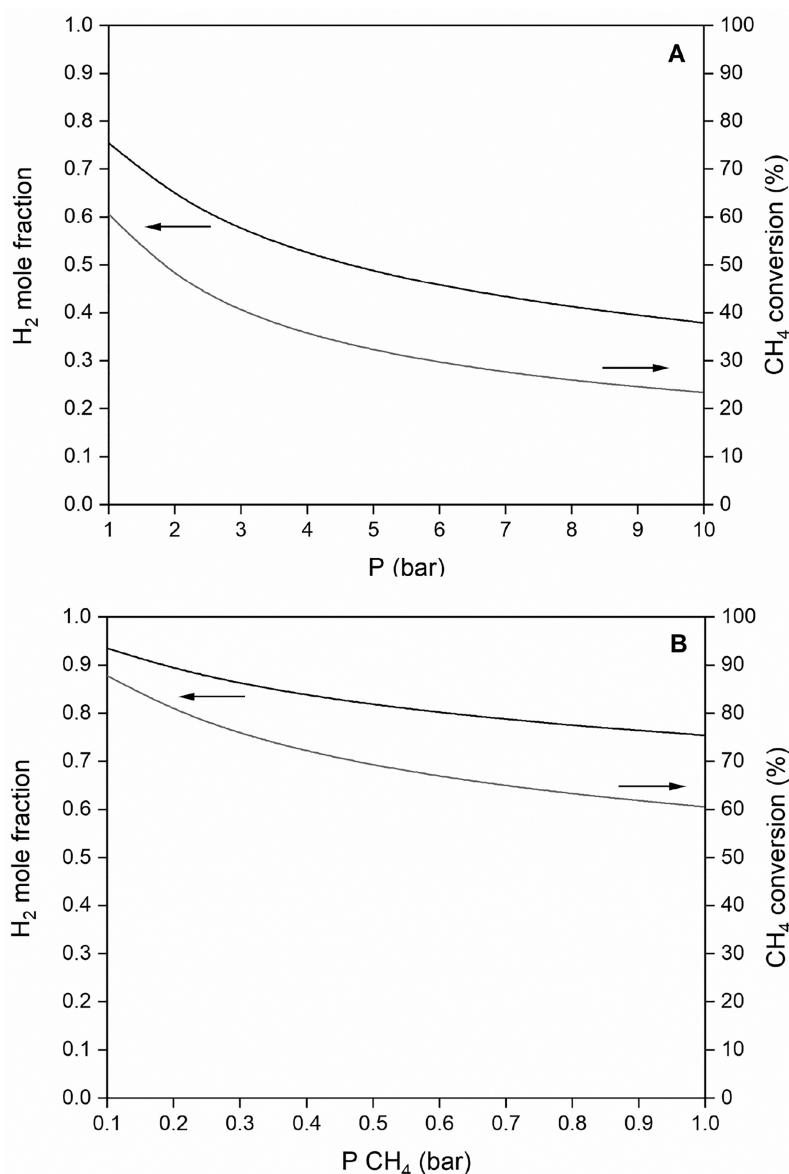


Figure 7. Hydrogen mole fraction (in the gas phase excluding carbon and nitrogen) and methane conversion in the thermodynamic equilibrium of methane pyrolysis at 600 °C at (A) different total pressures and (B) different methane partial pressures (total pressure = 1 bar, pressure balanced with nitrogen) (calculated using Aspen Plus software).

suitable experimental conditions for the implementation of an economic process on a large scale.

6. INDUSTRIALIZATION OF METHANE PYROLYSIS

The implementation of methane pyrolysis on an industrial scale requires the use of natural gas as a feed gas instead of pure methane. Research is usually limited to the use of methane as a single component, and the challenges associated with the operation with natural gas are not addressed in depth.⁴³ Therefore, the first issue to be elucidated is how the minor components of natural gas can affect the catalytic activity and stability. If they have a negative effect, a purification pretreatment will be necessary. Depending on the origin of natural gas, the minor compounds as well as their concentration may vary. Some of these impurities include ethane, propane, ethylene, H₂S, CO₂, and nitrogen.²⁵⁰ Experiments with mixtures simulating a natural gas composition (85% methane, 10% ethane, 5% propane) have been

carried out at 900 °C over carbon catalysts.²⁵⁰ The resulting gas product is only composed of unconverted methane and hydrogen, indicating the complete conversion of ethane and propane and the prevention of secondary gaseous products. In comparison to the experiments conducted with methane/nitrogen mixtures (85/15), the hydrogen concentration at the outlet improves using the simulated natural gas due to the additional hydrogen obtained from the decomposition of ethane and propane. The most important implication derived from this study is that the carbon product from these alkanes does not deactivate the carbon catalyst and the pyrolysis of methane is not negatively affected. Moreover, no extra purification post-treatments to remove ethane and propane are required since their decomposition is complete under such reaction conditions. However, it should be noted that a cleaning process may be necessary to remove possible minor compounds obtained as reaction intermediates. The presence of H₂S impurities in natural gas may also be favorable.^{250,251}

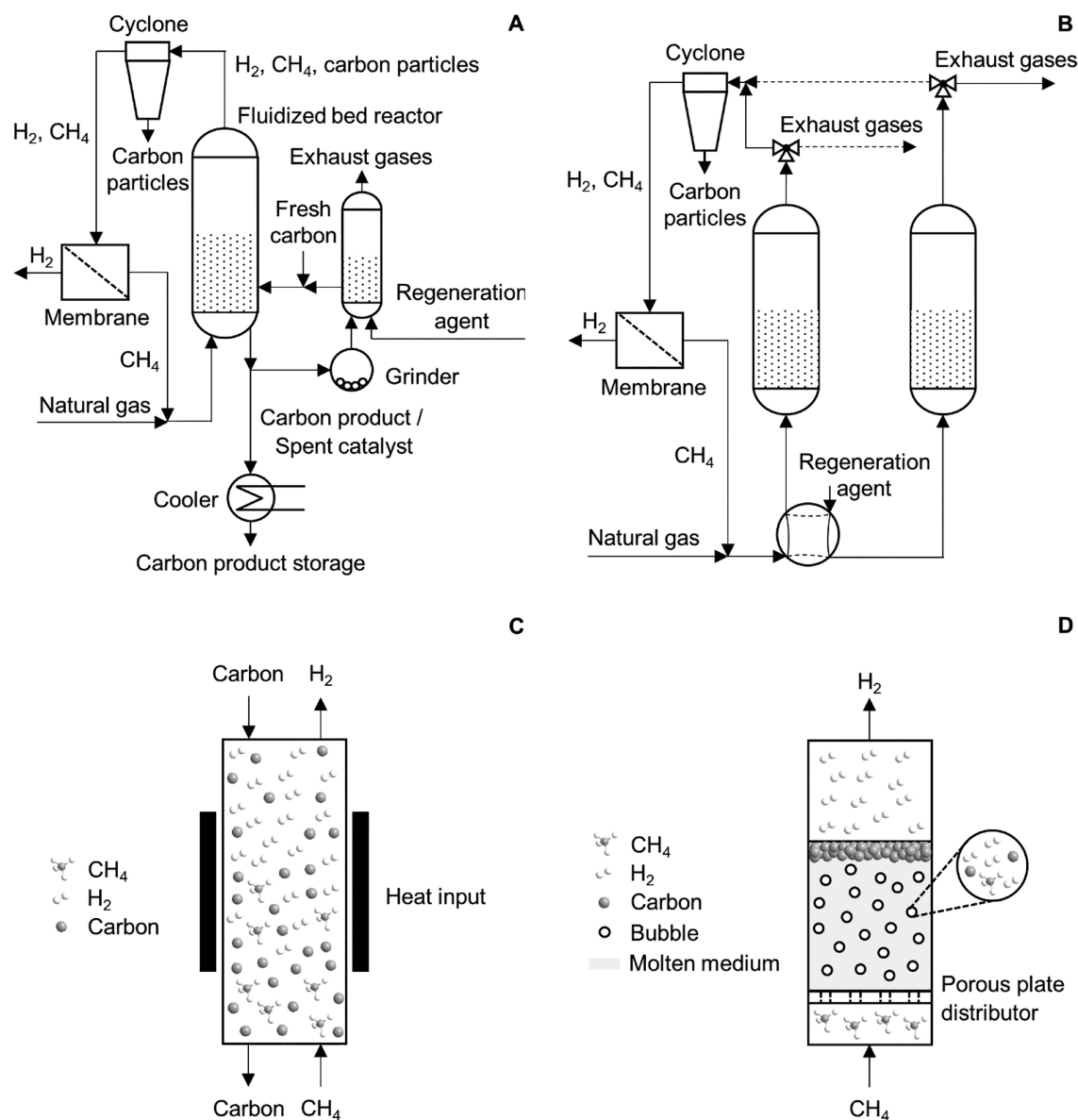


Figure 8. Potential reactor configurations for the industrial implementation of methane pyrolysis. (A) Fluidized-bed reactor with a catalyst regeneration unit according to refs 204 and 215. (B) Parallel reactors operating in a cyclic reaction-regeneration mode according to ref 199. (C) Moving-bed reactor according to ref 265. (D) Liquid bubble column reactor according to ref 263.

Carbon catalysts are not deactivated by small amounts of H₂S (up to ca. 1 vol %), but such impurities have a positive catalytic effect on the methane decomposition rate. The intermediate HS· radicals formed are able to attack methane molecules. This results in the formation of methyl radicals, which is followed by the stepwise decomposition to hydrogen and solid carbon. The resistance to H₂S deactivation is an important advantage of carbon materials over metal catalysts. Metal catalysts undergo severe deactivation in the presence of sulfur compounds and a purification treatment of natural gas becomes essential prior to the reaction.

6.1. Process Concepts for Industrial Application.

Concerning the technical implementation of methane pyrolysis on an industrial scale, different configurations may be possible, such as fluidized-bed reactors,²⁰⁴ moving-bed reactors,²⁵² or liquid bubble column reactors.^{29,31,253–263} Fixed-bed reactors are usually the preferred option on a laboratory scale. They are simple to operate and provide a better understanding of

catalyst performance, reaction kinetics, and the effect of different operating conditions.²⁶⁴ However, the main drawback is the filling of the reactor with the carbon product during long-term experiments. This increases the pressure drop and eventually blocks the gas flow.^{7,9}

Fluidized-bed reactors overcome this problem and provide additional advantages that are crucial for the industrial operation. For instance, a continuous addition and withdrawal of catalyst particles is possible in a fluidized-bed reactor. Therefore, the pressure drop does not increase significantly and the operation for longer times is possible. Additionally, the vigorous movement of the particles allows the efficient heat and mass transfer between the gas and the solid catalyst. Consequently, the temperature can be successfully controlled and the formation of hot spots is prevented.^{7,9} A potential configuration for the industrial operation with a carbon catalyst using a fluidized-bed reactor is presented in Figure 8A.^{204,215} Natural gas is introduced at the bottom of the reactor

containing the carbon catalyst particles. The outlet gas, which is composed of unconverted methane and hydrogen, is passed first through a cyclone to remove the possible entrained carbon particles. Afterward, the gaseous product stream flows through a membrane to separate methane and hydrogen. The recovered methane is recirculated and fed back to the reactor together with a fresh natural gas stream. The carbon catalyst and carbon deposits are collected at the reactor bottom, cooled, and stored. A small part of the carbon product can be introduced into the reactor after grinding and/or reactivation via a regeneration method. Another possible configuration consists of two parallel reactors (Figure 8B).¹⁹⁹ These reactors operate in a cyclic mode by switching the natural gas feed and the regeneration agent stream (air, steam) between the two reactors. Methane pyrolysis takes place in the first reactor, whereas the catalyst in the second reactor is regenerated. After a certain time natural gas is fed into the second reactor, where the pyrolysis occurs over a regenerated catalyst. In the same way, the regeneration agent is introduced in the first reactor to recover the activity of the corresponding spent catalyst. Therefore, the operation in both reactors alternates between methane pyrolysis and catalyst regeneration. Despite the promising results obtained after catalyst reactivation, the existing regeneration techniques result in undesirable CO_x emissions and should be avoided industrially. For this reason, the resulting carbon product should be intended for further applications or stored until other regeneration methods are available. In any case, obtaining a safe carbon product has to be guaranteed, and thus, toxic metal catalysts such as nickel or cobalt must be avoided. Iron and carbon catalysts are therefore the best choice to industrialize the pyrolysis process of methane.

An interesting reactor concept from the industrial point of view is the moving-bed reactor (Figure 8C) developed by different partners in a recent BMBF-funded joint project.²⁶⁵ In a moving-bed reactor natural gas and carbon granules flow in countercurrent throughout the reactor. Natural gas is fed at the bottom of the reactor, and carbon particles are fed at the top. The carbon is electrically heated by a direct current in the reaction zone. This heat is released and transferred to the feed gas. Consequently, the pyrolysis of methane takes place. The carbon originating from the reaction is accumulated on the carbon particles and continuously removed at the reactor bottom. The gaseous product is cooled down at the reactor top upon contact with the cold fresh carbon. As a consequence, the carbon is preheated by the outlet gas before entering the reaction zone and being electrically heated. The moving-bed reactor has important advantages. This kind of reactor provides a very good heat transfer between the gas and the solid catalyst. In addition, there is no back-mixing, and the residence time can be controlled for both phases. The counterflow operation allows the energy integration of the reactor, and the excellent heat transfer between the gas and the solid particles guarantees a thermally efficient process.²⁵² Although methane pyrolysis for hydrogen production is still not industrialized,⁴³ BASF plans to build a large-scale plant by 2030. They have investigated methane pyrolysis since 2010, and between 2013 and 2017 were part of the mentioned BMBF joint project based on a moving-bed reactor. Currently BASF is working on a test facility, the results of which will determine if methane pyrolysis can also succeed on an industrial scale.^{266,267}

A reactor design that is gaining importance for methane pyrolysis in recent years is the liquid bubble column reactor

(Figure 8D). This kind of reactor operates with molten media, such as molten metals (Ti, Pb, Sn, Ga), molten metal alloys (Ni–Bi, Cu–Bi) or molten salts (KBr, NaBr, NaCl, NaF, MnCl₂, KCl).^{29,31,253–263,268} Molten metals and salts act as heat transfer fluids^{254,256,259,263} and avoid temperature losses or gradients along the reactor.²⁶³ Furthermore, they could also serve as potential catalysts for the reaction.^{254,260,263} The main advantage of liquid bubble column reactors is the easy separation of the carbon byproduct from the liquid medium due to density differences.²⁹ Moreover, the low volatility and the solubility of carbon in liquids enable its deposition on the top of the molten medium and facilitate its separation and handling.²⁶³ The preferred liquid medium is based on molten metals since their density is very different from that of carbon, and thus, the carbon separation is more feasible.³¹ However, compared to molten metals, molten salts are less expensive, and are being further investigated in this field.²⁶³ The operation of liquid bubble column reactors is based on the formation of bubbles by the contact between the uprising methane gas and the liquid medium. The pyrolysis reaction occurs at the gas–liquid interface between the bubbles and the molten metal or salt. The bubbles ascend through the reactor and their size increases as a consequence of the molar expansion caused by the production of hydrogen and due to bubble coalescence. At the same time the resulting carbon is deposited at the gas–liquid interface. When the bubbles reach the surface of the molten medium, they open and release both, hydrogen and carbon. Hydrogen leaves the reactor, whereas carbon is accumulated in layers on top of the molten metal/salt bath. High residence times of the gas in the liquid and the use of a porous plate distributor are key parameters in the design of liquid bubble column reactors. The porous plate distributes homogeneously the gas phase along the reactor and produces small bubbles that increase the gas–liquid interfaces for the reaction, and consequently, the conversion of methane is improved.²⁶³ The constant removal of carbon from the liquid medium is possible in a bubble column configuration, so that blockage of the reactor due to carbon agglomeration is avoided.^{31,254,261} Additionally, the molten metal/salt is neither contaminated nor deactivated with the carbon product.^{29,260,262} This is an important advantage over solid catalysts. Solid catalysts deactivate, and to be reused a regeneration process to burn the carbon deposits is needed, which generates undesirable CO₂ emissions.²⁹ According to a life cycle assessment to evaluate the environmental impacts of the liquid-metal technology, the pyrolysis of methane could reduce the global warming impact by up to 64% compared to the steam reforming process.²⁶⁹ Although this technology bears good prospects for the future and may be competitive with steam methane reforming,²⁶³ the industrial scale implementation is still a challenge. One important drawback is the limited stability of the molten media at the required high operating temperatures (>900–1000 °C).³¹ Also, the corrosion at such high temperatures, especially in steel-based material reactors, limits the applicability of molten metals and salts.²⁵⁷

6.2. Perspectives of the Carbon Coproduct. The quality and sale of the carbon coproduct are aspects that may improve the economic efficiency of the industrial pyrolysis of methane. The characteristics of the carbon depend on the catalyst used and the reaction conditions. The formation of carbon nanotubes and nanofibers usually occurs over metal catalysts. At high operating temperatures the diameter and

length of the carbon nanofilaments decrease,^{125,130,131} and their crystallinity and graphitization degree increase.²³⁸ Carbons with different morphologies are obtained in carbon-catalyzed reactions. The morphology of carbon deposits over carbon materials depends on the catalyst nature. The formation of carbon blacks takes place over activated carbons, whereas carbon blacks produce amorphous turbostratic structures. The use of carbon nanotubes as a catalyst favors the growth of their walls, leading to the formation of multiwalled carbon nanotubes.¹⁴⁴ Carbon products derived from methane pyrolysis, such as carbon black, carbon fibers, and carbon nanotubes, have different applications and markets (Table 4).²⁷⁰ Carbon black is mainly composed of carbon

Table 4. Global Market and Price for Potential Carbon Products²⁷⁰

carbon product	global market (metric tons)	expected price (\$/ton)
carbon black	12,000,000 (2014)	400–2,000
	16,400,000 (2022)	
carbon fibers	70,000 (2016)	25,000–113,000
	100,000 (2020)	
carbon nanotubes	5,000 (2014)	100,000–600,000,000
	20,000 (2022)	

(≥97 wt %) in the form of colloidal particles. Approximately 90% of the total carbon black is used in rubber applications (as a filler and a strengthening/reinforcing agent in the manufacture of tires and other rubber and plastic products), 9% as a pigment (to enhance formulations and coatings) and the remaining 1% for diverse applications. Carbon black is also a valuable product for the metallurgical industry and can be used as a reducing agent for the production of SiC and as a carbon additive/carburizer in the steel industry.²⁰² Although the price of carbon black depends on its features, a range can be established depending on the quality and final use.²⁷⁰ For instance, the price of ASTM-grade carbon black for use in tires ranges from 400 \$ to over 1000 \$ per ton, whereas the price of specialty grade carbon black can exceed 2000 \$ per ton. The global demand for carbon black, which was nearly 12 million metric tons in 2014, is expected to increase up to 16.4 million metric tons by 2022. In the case of carbon fibers, they are polycrystalline, two-dimensional planar hexagonal networks of carbon containing 92–100% carbon by weight. They have applications in many fields, such as aerospace, automobiles, carbon-reinforced composite materials and textiles. Carbon nanofibers are also used as hydrogen storage materials and have applications in nanoelectrical devices, nanowires, and nanosensors.¹⁵¹ The global market demand for carbon fibers was 70 000 t in 2016 and is projected to exceed 100 000 t in 2020.²⁷⁰ Carbon nanotubes (single-walled and multiwalled carbon nanotubes) find applications in polymers, electronics, plastics, and energy storage. They are mostly intended to improve the thermal, electrical, and mechanical properties of polymers, although they are getting special attention for their applications in lithium-ion batteries and renewable energy storage. The global market demand for carbon nanotubes was slightly over 5000 tons in 2014 and is projected to surpass 20 000 tons by 2022.²⁷⁰

The commercialization of the carbon byproduct may positively influence the economics of the global process by reducing the hydrogen costs. This would be possible if the global market could absorb the huge amounts of the carbon

product resulting from the pyrolysis process to meet the corresponding hydrogen demand.²⁷⁰ If the annual global production of hydrogen (ca. 60 million tons in 2017) comes from methane pyrolysis, close to 180 million tons of carbon would be generated.²⁷¹ From a different point of view, if only the hydrogen production from steam methane reforming (ca. 48% of the total hydrogen production) is replaced by methane pyrolysis, approximately 86 million tons of carbon would be obtained yearly.²⁶³ Since the current world consumption of all carbon products is only 15–20 million tons per year,²⁷¹ in none of the previous cases would the market be able to accommodate such amounts of carbon. The only realistic application for such quantities of carbon is its use in the area of soil amendment and environmental remediation, although its suitability has yet to be proven.²⁷ The use of carbon for the amelioration of soil may accommodate large amounts of carbon²⁸ and provide a virtually unlimited market for the methane pyrolysis carbon coproduct.²⁷ The addition of carbonaceous products to soil can significantly improve seed germination, plant growth and crop yields. The application of carbon to soil increases the nutrient and water retention capacity as well as the microbial abundance. Carbon can store nutrients from the soil and serve as a potential slow-release fertilizer. For this reason, the amount of fertilizers applied to soil could be significantly decreased. Furthermore, the addition of carbon to soil may reduce the CO₂ in the atmosphere by enhancing its sequestration and by reducing the CO₂ emissions from the soil to the environment. Therefore, carbon would act as a long-term CO₂ sink.^{23,27} The structure of the amorphous carbons obtained in methane pyrolysis under certain operating conditions is similar to that of the carbons commonly used for soil amendment, and thus, they are expected to have a positive effect on plant growth. Nevertheless, further investigations are required to validate the suitability of the carbon coproduct of methane pyrolysis for soil amendment and environmental cleanup.²⁷ The application in this area requires that the carbon from the decomposition of methane is not poisoned with toxic metals, such as nickel or cobalt. Consequently, the use of iron and carbon catalysts is the only possibility to obtain a carbon product free of harmful compounds with a potential application for soil improvement and environmental remediation. Carbon storage as a back-up energy source for the future is another alternative solution for the carbon byproduct.²⁶³ Unlike the CO₂ capture and sequestration systems required in the steam methane reforming process, no significant energy consumption is expected from carbon storage.²¹⁵ Furthermore, for the same hydrogen production the volume required for the storage of CO₂ in liquid form obtained via SMR would be 10 times larger than the volume needed to store the carbon produced by methane pyrolysis.²²

Methane pyrolysis has a good outlook for future as a zero-emission technology for hydrogen production. Nevertheless, at present there are still many open questions for its industrial implementation. For instance, the role of the impurities of natural gas in the catalytic performance needs to be unraveled. In addition, a suitable experimental setup must still be found to industrialize the process, and the possible commercialization or storage of the carbon product, as well as its impact on the economics of the process, must be ascertained.

7. CONCLUSIONS


The present strict regulations to reduce greenhouse gas emissions are forcing the development of a sustainable low-

carbon economy. In this context, hydrogen plays a key role in the transition to clean energy. Hydrogen has received special attention as a zero-emission fuel in fuel cells and internal combustion engines. In addition, hydrogen is essential for converting industrial CO₂ emissions into platform chemicals such as methanol, which prevents CO₂ from being released into the atmosphere. Most of the current global hydrogen production comes from coal gasification and steam methane reforming. However, both processes are accompanied by large CO₂ emissions and must be avoided to comply with restrictions on GHG emissions. Water electrolysis based on renewable energies is the greenest technology for hydrogen production, but the total dependence on renewables is not possible, at least, in the near future. Consequently, alternative fossil fuel-based processes with a low carbon footprint become essential. Methane pyrolysis is a suitable technology for converting natural gas into hydrogen without CO₂ emissions. Although methane pyrolysis is not a sustainable process due to the depletion of natural gas reserves, it can be an appropriate temporary solution until renewable energies are well established. The decomposition of methane has been extensively studied over different metal (Ni, Co, Fe) and carbon catalysts. From an industrial point of view, only the use of iron and carbon catalysts is viable due to their nontoxicity. This allows a safe storage of the carbon product or its potential application, for example, for soil amendment and environmental remediation. Nevertheless, severe temperatures are required to obtain satisfying hydrogen yields over iron and carbon catalysts. Although the reaction mechanism has been widely investigated, no clear conclusions have been drawn on the elementary reactions and the rate-limiting step. Therefore, further research is needed to elucidate these issues. This will enable the development of suitable catalysts to optimize the activity under milder operating conditions. Furthermore, the role of natural gas impurities in the production of hydrogen has to be investigated in more detail. Finding an adequate reactor configuration and a thorough understanding of how the sale of the carbon product may affect the economics of the process are additional issues that will determine the industrial implementation. Although the industrialization of methane pyrolysis still has to overcome many challenges, this CO₂-free technology is a promising process that can serve as a bridge in the evolution toward a sustainable hydrogen production based on renewable energies.

AUTHOR INFORMATION

Corresponding Authors

Nuria Sánchez-Bastardo – Max Planck Institute for Chemical Energy Conversion, 45470 Mülheim an der Ruhr, Germany;
Email: nuria.sanchez-bastardo@cec.mpg.de

Holger Ruland – Max Planck Institute for Chemical Energy Conversion, 45470 Mülheim an der Ruhr, Germany;
 orcid.org/0000-0001-5530-1458;
Email: holger.ruland@cec.mpg.de

Author

Robert Schlögl – Max Planck Institute for Chemical Energy Conversion, 45470 Mülheim an der Ruhr, Germany; Max Planck Society, Fritz Haber Institute, 14195 Berlin, Germany

Complete contact information is available at:
<https://pubs.acs.org/10.1021/acs.iecr.1c01679>

Funding

Bundesministerium für Bildung und Forschung, BMBF, Verbundvorhaben Carbon2Chem, support code: 03EK3037C. Open access funded by Max Planck Society.

Notes

The authors declare no competing financial interest.

ACKNOWLEDGMENTS

The authors would like to thank the Max Planck Society for financial support as well as the Federal Ministry of Education and Research (Bundesministerium für Bildung und Forschung, BMBF, Verbundvorhaben Carbon2Chem, support code: 03EK3037C) for funding.

ABBREVIATIONS

BMBF = Bundesministeriums für Bildung und Forschung
CCS = carbon capture and storage
ETEM = environmental transmission electron microscopy
GHG = greenhouse gas
GHSV = gas hourly space velocity
HES = high-energy sites
HREELS = high-resolution electron energy loss spectroscopy
NIST = National Institute of Standards and Technology
SMR = steam methane reforming
TEM = Transmission electron microscopy
VLS = vapor–liquid–solid
WGS = water-gas shift
XPS = X-ray photoelectron spectroscopy
XRD = X-ray diffraction

REFERENCES

- (1) *Paris Agreement to the United Nations Framework Convention on Climate Change*; United Nations, Paris, 2015.
- (2) *Kyoto Protocol to the United Nations Framework Convention on Climate Change*; United Nations, Kyoto, 1997.
- (3) <https://www.umweltbundesamt.de/daten/klima/treibhausgas-emissionen-in-deutschland#emissionsentwicklung> (accessed 2021-03-18).
- (4) *CO₂ emissions from fuel combustion. Highlights*; International Energy Agency, 2018.
- (5) Viswanathan, B. *Hydrogen as an energy carrier Energy Sources: Fundamentals of chemical conversion processes and applications*; Elsevier Science Bv: Amsterdam, 2017.
- (6) Ashik, U. P. M.; Daud, W. M. A. W.; Abbas, H. F. Production of greenhouse gas free hydrogen by thermocatalytic decomposition of methane - A review. *Renewable Sustainable Energy Rev.* **2015**, *44*, 221–256.
- (7) Abbas, H. F.; Daud, W. M. A. W. Hydrogen production by methane decomposition: A review. *Int. J. Hydrogen Energy* **2010**, *35* (3), 1160–1190.
- (8) Karchiyappan, T. A review on hydrogen energy production from electrochemical system: Benefits and challenges. *Energy Sources, Part A* **2019**, *41* (7), 902–909.
- (9) Zhang, J. B.; Li, X.; Chen, H. Y.; Qi, M.; Zhang, G. R.; Hu, H. Q.; Ma, X. X. Hydrogen production by catalytic methane decomposition: Carbon materials as catalysts or catalyst supports. *Int. J. Hydrogen Energy* **2017**, *42* (31), 19755–19775.
- (10) Younessi-Sinaki, M.; Matida, E. A.; Hamdullahpur, F. Kinetic model of homogeneous thermal decomposition of methane and ethane. *Int. J. Hydrogen Energy* **2009**, *34* (9), 3710–3716.
- (11) Zhang, J. B.; Li, X.; Xie, W. T.; Hao, Q. Q.; Chen, H. Y.; Ma, X. X. K₂CO₃-promoted methane pyrolysis on nickel/coal-char hybrids. *J. Anal. Appl. Pyrolysis* **2018**, *136*, 53–61.

- (12) Deerberg, G.; Oles, M.; Schlögl, R. The Project Carbon2-Chem®. *Chem. Ing. Tech.* **2018**, *90* (10), 1365–1368.
- (13) Schittkowski, J.; Ruland, H.; Laudenschleger, D.; Girod, K.; Kähler, K.; Kaluza, S.; Muhler, M.; Schlögl, R. Methanol synthesis from steel mill exhaust gases: Challenges for the industrial Cu/ZnO/Al₂O₃ catalyst. *Chem. Ing. Tech.* **2018**, *90* (10), 1419–1429.
- (14) Dawood, F.; Anda, M.; Shafiqullah, G. M. Hydrogen production for energy: An overview. *Int. J. Hydrogen Energy* **2020**, *45* (7), 3847–3869.
- (15) *BP Energy Outlook: 2019 ed.*; BP p.l.c.: London, 2019.
- (16) Eerkens, J. W. *The nuclear imperative: A critical look at the approaching energy crisis*, 2nd ed.; Springer: Dordrecht, 2010.
- (17) Grosspietsch, D.; Saenger, M.; Girod, B. Matching decentralized energy production and local consumption: A review of renewable energy systems with conversion and storage technologies. *Wiley Interdiscip. Rev.: Energy Environ.* **2019**, *8* (4), 18.
- (18) <https://www.bdew.de/service/daten-und-grafiken/jahresvolllaststunden/> (accessed 2021-03-18).
- (19) O'Dwyer, C.; Ryan, L.; Flynn, D. Efficient large-scale energy storage dispatch: Challenges in future high renewable systems. *IEEE Trans. Power Syst.* **2017**, *32* (5), 3439–3450.
- (20) Abdalla, A. M.; Hossain, S.; Nisfindy, O. B.; Azad, A. T.; Dawood, M.; Azad, A. K. Hydrogen production, storage, transportation and key challenges with applications: A review. *Energy Convers. Manage.* **2018**, *165*, 602–627.
- (21) Weger, L.; Abánades, A.; Butler, T. Methane cracking as a bridge technology to the hydrogen economy. *Int. J. Hydrogen Energy* **2017**, *42* (1), 720–731.
- (22) Abánades, A. In *Production of Hydrogen from Renewable Resources*; Fang, Z.; Smith, J. R. L.; Qi, X., Eds.; Springer: Dordrecht, 2015.
- (23) Muradov, N. Z.; Veziroğlu, T. N. Green[®] path from fossil-based to hydrogen economy: An overview of carbon-neutral technologies. *Int. J. Hydrogen Energy* **2008**, *33* (23), 6804–6839.
- (24) Abánades, A.; Rubbia, C.; Salmieri, D. Technological challenges for industrial development of hydrogen production based on methane cracking. *Energy* **2012**, *46* (1), 359–363.
- (25) Keipi, T.; Hankalin, V.; Nummelin, J.; Raiko, R. Techno-economic analysis of four concepts for thermal decomposition of methane: Reduction of CO₂ emissions in natural gas combustion. *Energy Convers. Manage.* **2016**, *110*, 1–12.
- (26) Parkinson, B.; Tabatabaei, M.; Upham, D. C.; Ballinger, B.; Greig, C.; Smart, S.; McFarland, E. Hydrogen production using methane: Techno-economics of decarbonizing fuels and chemicals. *Int. J. Hydrogen Energy* **2018**, *43* (5), 2540–2555.
- (27) Muradov, N. Z.; Veziroğlu, T. N. From hydrocarbon to hydrogen-carbon to hydrogen economy. *Int. J. Hydrogen Energy* **2005**, *30* (3), 225–237.
- (28) Steinberg, M. Fossil fuel decarbonization technology for mitigating global warming. *Int. J. Hydrogen Energy* **1999**, *24* (8), 771–777.
- (29) Kang, D.; Palmer, C.; Mannini, D.; Rahimi, N.; Gordon, M. J.; Metiu, H.; McFarland, E. W. Catalytic methane pyrolysis in molten alkali chloride salts containing iron. *ACS Catal.* **2020**, *10* (13), 7032–7042.
- (30) Machhammer, O.; Bode, A.; Hormuth, W. Financial and ecological evaluation of hydrogen production processes on large scale. *Chem. Eng. Technol.* **2016**, *39* (6), 1185–1193.
- (31) Abánades, A.; Rubbia, C.; Salmieri, D. Thermal cracking of methane into hydrogen for a CO₂-free utilization of natural gas. *Int. J. Hydrogen Energy* **2013**, *38* (20), 8491–8496.
- (32) Dufour, J.; Serrano, D. P.; Galvez, J. L.; Moreno, J.; Garcia, C. Life cycle assessment of processes for hydrogen production. Environmental feasibility and reduction of greenhouse gases emissions. *Int. J. Hydrogen Energy* **2009**, *34* (3), 1370–1376.
- (33) Fidalgo, B.; Menéndez, J. A. Carbon materials as catalysts for decomposition and CO₂ reforming of methane: A review. *Chin. J. Catal.* **2011**, *32* (2), 207–216.
- (34) Richardson, Y.; Drobek, M.; Julbe, A.; Blin, J.; Pinta, F. In *Recent Advances in Thermochemical Conversion of Biomass*; Pandey, A., Bhaskar, T., Stöcker, M., Sukumaran, R. K., Eds.; Elsevier: Amsterdam, 2015.
- (35) Lu, Y. J.; Zhu, L. Y.; Agrafiotis, C.; Vieten, J.; Roeb, M.; Sattler, C. Solar fuels production: Two-step thermochemical cycles with cerium-based oxides. *Prog. Energy Combust. Sci.* **2019**, *75*, 49.
- (36) Chi, J.; Yu, H. M. Water electrolysis based on renewable energy for hydrogen production. *Chin. J. Catal.* **2018**, *39* (3), 390–394.
- (37) El-Emam, R. S.; Özcan, H. Comprehensive review on the techno-economics of sustainable large-scale clean hydrogen production. *J. Cleaner Prod.* **2019**, *220*, 593–609.
- (38) Von Wald, G. A.; Masnadi, M. S.; Upham, D. C.; Brandt, A. R. Optimization-based technoeconomic analysis of molten-media methane pyrolysis for reducing industrial sector CO₂ emissions. *Sustainable Energy Fuels* **2020**, *4* (9), 4598–4613.
- (39) Laugs, G. A. H.; Benders, R. M. J.; Moll, H. C. Balancing responsibilities: Effects of growth of variable renewable energy, storage, and undue grid interaction. *Energy Policy* **2020**, *139*, 111203.
- (40) Kalamaras, C. M.; Efstathiou, A. M. Hydrogen production technologies: Current state and future developments. *Conference Papers in Energy* **2013**, *2013*, 690627.
- (41) Pinsky, R.; Sabharwall, P.; Hartvigsen, J.; O'Brien, J. Comparative review of hydrogen production technologies for nuclear hybrid energy systems. *Prog. Nucl. Energy* **2020**, *123*, 103317.
- (42) Pudukudy, M.; Yaakob, Z.; Jia, Q. M.; Takriff, M. S. Catalytic decomposition of undiluted methane into hydrogen and carbon nanotubes over Pt promoted Ni/CeO₂ catalysts. *New J. Chem.* **2018**, *42* (18), 14843–14856.
- (43) Schneider, S.; Bajohr, S.; Graf, F.; Kolb, T. State of the art of hydrogen production via pyrolysis of natural gas. *ChemBioEng Rev.* **2020**, *7* (5), 150–158.
- (44) Blanksby, S. J.; Ellison, G. B. Bond dissociation energies of organic molecules. *Acc. Chem. Res.* **2003**, *36* (4), 255–263.
- (45) Skinner, G. B.; Ruehrwein, R. A. Shock tube studies on the pyrolysis and oxidation of methane. *J. Phys. Chem.* **1959**, *63* (10), 1736–1742.
- (46) Kevorkian, V.; Heath, C. E.; Boudart, M. The decomposition of methane in shock waves. *J. Phys. Chem.* **1960**, *64* (8), 964–968.
- (47) Kozlov, G. I.; Knorre, V. G. Single-pulse shock tube studies on kinetics of thermal decomposition of methane. *Combust. Flame* **1962**, *6* (4), 253–263.
- (48) Yano, T.; Kuratani, K. Initiation step of methane pyrolysis. *Bull. Chem. Soc. Jpn.* **1968**, *41* (4), 799–802.
- (49) Napier, D. H.; Subrahmanyam, N. Pyrolysis of methane in a single pulse shock tube. *J. Appl. Chem. Biotechnol.* **1972**, *22* (3), 303–317.
- (50) Palmer, H. B.; Lahaye, J.; Hou, K. C. Kinetics and mechanism of the thermal decomposition of methane in a flow system. *J. Phys. Chem.* **1968**, *72* (1), 348–353.
- (51) Yano, T. Initiation step of methane pyrolysis. Further studies on initiation step of methane pyrolysis. *Bull. Chem. Soc. Jpn.* **1973**, *46* (6), 1619–1623.
- (52) Chen, C.-J.; Back, M. H.; Back, R. A. The thermal decomposition of methane. I. Kinetics of the primary decomposition to C₂H₆ + H₂; rate constant for the homogeneous unimolecular dissociation of methane and its pressure dependence. *Can. J. Chem.* **1975**, *53* (23), 3580–3590.
- (53) Chen, C.-J.; Back, M. H.; Back, R. A. The thermal decomposition of methane. II. Secondary reactions, autocatalysis and carbon formation; non-Arrhenius behaviour in the reaction of CH₃ with ethane. *Can. J. Chem.* **1976**, *54* (20), 3175–3184.
- (54) Chen, C.-J.; Back, M. H.; Back, R. A. Mechanism of the Thermal Decomposition of Methane. *ACS Symposium Series* **1976**, *32*, 1 DOI: 10.1021/bk-1976-0032.ch001.
- (55) Roscoe, J. M.; Thompson, M. J. Thermal decomposition of methane: Autocatalysis. *Int. J. Chem. Kinet.* **1985**, *17* (9), 967–990.
- (56) Benzinger, W.; Becker, A.; Hüttinger, K. J. Chemistry and kinetics of chemical vapour deposition of pyrocarbon: I. Fundamen-

tals of kinetics and chemical reaction engineering. *Carbon* **1996**, *34* (8), 957–966.

(57) Khan, M. S.; Crynes, B. L. Survey of recent methane pyrolysis literature. *Ind. Eng. Chem.* **1970**, *62* (10), 54–59.

(58) Grabke, H. J. Evidence on the surface concentration of carbon on gamma iron from the kinetics of the carburization in CH₄-H₂. *Metall. Trans.* **1970**, *1* (10), 2972–2975.

(59) Snoeck, J.-W.; Froment, G. F.; Fowles, M. Kinetic study of the carbon filament formation by methane cracking on a nickel catalyst. *J. Catal.* **1997**, *169* (1), 250–262.

(60) Sharif Zein, S. H.; Mohamed, A. R.; Talpa Sai, P. S. Kinetic studies on catalytic decomposition of methane to hydrogen and carbon over Ni/TiO₂ catalyst. *Ind. Eng. Chem. Res.* **2004**, *43* (16), 4864–4870.

(61) Zavarukhin, S. G.; Kuvshinov, G. G. The kinetic model of formation of nanofibrous carbon from CH₄-H₂ mixture over a high-loaded nickel catalyst with consideration for the catalyst deactivation. *Appl. Catal., A* **2004**, *272* (1), 219–227.

(62) Suelves, L.; Pinilla, J. L.; Lázaro, M. J.; Moliner, R.; Palacios, J. M. Effects of reaction conditions on hydrogen production and carbon nanofiber properties generated by methane decomposition in a fixed bed reactor using a NiCuAl catalyst. *J. Power Sources* **2009**, *192* (1), 35–42.

(63) Saraswat, S. K.; Sinha, B.; Pant, K. K.; Gupta, R. B. Kinetic study and modeling of homogeneous thermocatalytic decomposition of methane over a Ni-Cu-Zn/Al₂O₃ catalyst for the production of hydrogen and bamboo-shaped carbon nanotubes. *Ind. Eng. Chem. Res.* **2016**, *55* (45), 11672–11680.

(64) Alstrup, I.; Tavares, M. T. The kinetics of carbon formation from CH₄ + H₂ on a silica-supported nickel catalyst. *J. Catal.* **1992**, *135* (1), 147–155.

(65) Alstrup, I.; Tavares, M. T. Kinetics of carbon formation from CH₄ + H₂ on silica-supported nickel and Ni-Cu catalysts. *J. Catal.* **1993**, *139* (2), 513–524.

(66) Zadeh, J. S. M.; Smith, K. J. Kinetics of CH₄ decomposition on supported cobalt catalysts. *J. Catal.* **1998**, *176* (1), 115–124.

(67) Zhang, Y.; Smith, K. J. A kinetic model of CH₄ decomposition and filamentous carbon formation on supported Co catalysts. *J. Catal.* **2005**, *231* (2), 354–364.

(68) Muradov, N.; Smith, F.; T-Raissi, A. Catalytic activity of carbons for methane decomposition reaction. *Catal. Today* **2005**, *102–103*, 225–233.

(69) Serrano, D. P.; Botas, J. A.; Fierro, J. L. G.; Guil-López, R.; Pizarro, P.; Gómez, G. Hydrogen production by methane decomposition: Origin of the catalytic activity of carbon materials. *Fuel* **2010**, *89* (6), 1241–1248.

(70) Douven, S.; Pirard, S. L.; Heyen, G.; Toye, D.; Pirard, J.-P. Kinetic study of double-walled carbon nanotube synthesis by catalytic chemical vapour deposition over an Fe-Mo/MgO catalyst using methane as the carbon source. *Chem. Eng. J.* **2011**, *175*, 396–407.

(71) Yeheskel, J.; Epstein, M. Thermolysis of methane in a solar reactor for mass-production of hydrogen and carbon nano-materials. *Carbon* **2011**, *49* (14), 4695–4703.

(72) Yadav, M. D.; Dasgupta, K.; Patwardhan, A. W.; Kaushal, A.; Joshi, J. B. Kinetic study of single-walled carbon nanotube synthesis by thermocatalytic decomposition of methane using floating catalyst chemical vapour deposition. *Chem. Eng. Sci.* **2019**, *196*, 91–103.

(73) Yadav, M. D.; Patwardhan, A. W.; Joshi, J. B.; Dasgupta, K. Kinetic study of multi-walled carbon nanotube synthesis by thermocatalytic decomposition of methane using floating catalyst chemical vapour deposition. *Chem. Eng. J.* **2019**, *377*, 119895.

(74) Wang, J.; Li, X.; Zhou, Y.; Yu, G.; Jin, L.; Hu, H. Mechanism of methane decomposition with hydrogen addition over activated carbon via in-situ pyrolysis-electron impact ionization time-of-flight mass spectrometry. *Fuel* **2020**, *263*, 116734.

(75) Chen, Q.; Lua, A. C. Kinetic reaction and deactivation studies on thermocatalytic decomposition of methane by electroless nickel plating catalyst. *Chem. Eng. J.* **2020**, *389*, 124366.

(76) Ceyer, S. T.; Yang, Q. Y.; Lee, M. B.; Beckerle, J. D.; Johnson, A. D. In *Studies in Surface Science and Catalysis*; Bibby, D. M.; Chang, C. D.; Howe, R. F.; Yurchak, S., Eds.; Elsevier: Amsterdam, 1988.

(77) Lee, M. B.; Yang, Q. Y.; Tang, S. L.; Ceyer, S. T. Activated dissociative chemisorption of CH₄ on Ni(111): Observation of a methyl radical and implication for the pressure gap in catalysis. *J. Chem. Phys.* **1986**, *85* (3), 1693–1694.

(78) Lee, M. B.; Yang, Q. Y.; Ceyer, S. T. Dynamics of the activated dissociative chemisorption of CH₄ and implication for the pressure gap in catalysis: A molecular beam–high resolution electron energy loss study. *J. Chem. Phys.* **1987**, *87* (5), 2724–2741.

(79) Wagner, R. S.; Ellis, W. C. Vapor-Liquid-Solid mechanism of single crystal growth. *Appl. Phys. Lett.* **1964**, *4* (5), 89–90.

(80) Baker, R. T. K.; Barber, M. A.; Harris, P. S.; Feates, F. S.; Waite, R. J. Nucleation and growth of carbon deposits from the nickel catalyzed decomposition of acetylene. *J. Catal.* **1972**, *26* (1), 51–62.

(81) Baker, R. T. K. Catalytic growth of carbon filaments. *Carbon* **1989**, *27* (3), 315–323.

(82) Baker, R. T. K.; Harris, P. S.; Thomas, R. B.; Waite, R. J. Formation of filamentous carbon from iron, cobalt and chromium catalyzed decomposition of acetylene. *J. Catal.* **1973**, *30* (1), 86–95.

(83) Rostrup-Nielsen, J. R.; Trimm, D. L. Mechanisms of carbon formation on nickel-containing catalysts. *J. Catal.* **1977**, *48* (1), 155–165.

(84) Snoeck, J. W.; Froment, G. F.; Fowles, M. Filamentous carbon formation and gasification: Thermodynamics, driving force, nucleation, and steady-state growth. *J. Catal.* **1997**, *169* (1), 240–249.

(85) Klinke, C.; Bonard, J.-M.; Kern, K. Thermodynamic calculations on the catalytic growth of multiwall carbon nanotubes. *Phys. Rev. B: Condens. Matter Mater. Phys.* **2005**, *71* (3), 035403.

(86) Baird, T.; Fryer, J. R.; Grant, B. Carbon formation on iron and nickel foils by hydrocarbon pyrolysis—reactions at 700°C. *Carbon* **1974**, *12* (5), 591–602.

(87) Oberlin, A.; Endo, M.; Koyama, T. Filamentous growth of carbon through benzene decomposition. *J. Cryst. Growth* **1976**, *32* (3), 335–349.

(88) Helveg, S.; López-Cartes, C.; Sehested, J.; Hansen, P. L.; Clausen, B. S.; Rostrup-Nielsen, J. R.; Abild-Pedersen, F.; Nørskov, J. K. Atomic-scale imaging of carbon nanofibre growth. *Nature* **2004**, *427* (6973), 426–429.

(89) Hofmann, S.; Csányi, G.; Ferrari, A. C.; Payne, M. C.; Robertson, J. Surface diffusion: The low activation energy path for nanotube growth. *Phys. Rev. Lett.* **2005**, *95* (3), No. 036101, DOI: 10.1103/PhysRevLett.95.036101.

(90) Raty, J.-Y.; Gygi, F.; Galli, G. Growth of carbon nanotubes on metal nanoparticles: A microscopic mechanism from ab initio molecular dynamics simulations. *Phys. Rev. Lett.* **2005**, *95*, 096103.

(91) Rinaldi, A.; Tessonier, J.-P.; Schuster, M. E.; Blume, R.; Girgsdies, F.; Zhang, Q.; Jacob, T.; Hamid, S. B. A.; Su, D. S.; Schlögl, R. Dissolved carbon controls the initial stages of nanocarbon growth. *Angew. Chem., Int. Ed.* **2011**, *50* (14), 3313–3317.

(92) Kumar, M. *Carbon nanotube synthesis and growth mechanism Carbon Nanotubes - Synthesis, Characterization, Applications*; IntechOpen: Rijeka, Croatia, 2011.

(93) Kutteri, D. A.; Wang, I.-W.; Samanta, A.; Li, L. L.; Hu, J. L. Methane decomposition to tip and base grown carbon nanotubes and CO_x-free H₂ over mono- and bimetallic 3d transition metal catalysts. *Catal. Sci. Technol.* **2018**, *8* (3), 858–869.

(94) Wang, I.-W.; Kutteri, D. A.; Gao, B. Y.; Tian, H. J.; Hu, J. L. Methane pyrolysis for carbon nanotubes and CO_x-Free H₂ over transition-metal catalysts. *Energy Fuels* **2019**, *33* (1), 197–205.

(95) Kharlamova, M. V. Investigation of growth dynamics of carbon nanotubes. *Beilstein J. Nanotechnol.* **2017**, *8*, 826–856.

(96) Chesnokov, V. V.; Buyanov, R. A. Mechanism for the formation of carbon deposits from benzene on iron and nickel. *Kinet. Catal.* **1987**, *28* (2), 353–357.

(97) Chesnokov, V. V.; Buyanov, R. A. The formation of carbon filaments upon decomposition of hydrocarbons catalysed by iron

subgroup metals and their alloys. *Russ. Chem. Rev.* **2000**, *69* (7), 623–638.

(98) Zaikovskii, V. I.; Chesnokov, V. V.; Buyanov, R. A. The relationship between the state of active species in a Ni/Al₂O₃ catalyst and the mechanism of growth of filamentous carbon. *Kinet. Catal.* **2001**, *42* (6), 813–820.

(99) Buyanov, R. A.; Chesnokov, V. V. On the processes that occur in the metal particles with their use in catalytic decomposition of hydrocarbons through the carbide cycle mechanism. *Chem. Sustainable Dev.* **2005**, *13*, 37–40.

(100) Ni, L.; Kuroda, K.; Zhou, L.-P.; Ohta, K.; Matsuishi, K.; Nakamura, J. Decomposition of metal carbides as an elementary step of carbon nanotube synthesis. *Carbon* **2009**, *47* (13), 3054–3062.

(101) Esconjauregui, S.; Whelan, C. M.; Maex, K. The reasons why metals catalyze the nucleation and growth of carbon nanotubes and other carbon nanomorphologies. *Carbon* **2009**, *47* (3), 659–669.

(102) Narkiewicz, U.; Podsiadly, M.; Jędrzejewski, R.; Pelech, I. Catalytic decomposition of hydrocarbons on cobalt, nickel and iron catalysts to obtain carbon nanomaterials. *Appl. Catal., A* **2010**, *384* (1), 27–35.

(103) Podsiadly, M.; Pelech, I.; Narkiewicz, U. Synthesis of nanocrystalline nickel and iron carbides by decomposition of hydrocarbons. *Mater. Sci.-Pol.* **2013**, *31* (1), 65–70.

(104) Wirth, C. T.; Hofmann, S.; Robertson, J. State of the catalyst during carbon nanotube growth. *Diamond Relat. Mater.* **2009**, *18* (5–8), 940–945.

(105) Weatherup, R. S.; Bayer, B. C.; Blume, R.; Ducati, C.; Baetz, C.; Schlögl, R.; Hofmann, S. In situ characterization of alloy catalysts for low-temperature graphene growth. *Nano Lett.* **2011**, *11* (10), 4154–4160.

(106) Weatherup, R. S.; Bayer, B. C.; Blume, R.; Baetz, C.; Kidambi, P. R.; Fouquet, M.; Wirth, C. T.; Schlögl, R.; Hofmann, S. On the mechanisms of Ni-catalysed graphene chemical vapour deposition. *ChemPhysChem* **2012**, *13* (10), 2544–2549.

(107) Alstrup, I. A new model explaining carbon filament growth on nickel, iron, and Ni-Cu alloy catalysts. *J. Catal.* **1988**, *109* (2), 241–251.

(108) Emmenegger, C.; Bonard, J. M.; Mauron, P.; Sudan, P.; Lepora, A.; Grobety, B.; Züttel, A.; Schlapbach, L. Synthesis of carbon nanotubes over Fe catalyst on aluminium and suggested growth mechanism. *Carbon* **2003**, *41* (3), 539–547.

(109) Pérez-Cabero, M.; Rodríguez-Ramos, I.; Guerrero-Ruñz, A. Characterization of carbon nanotubes and carbon nanofibers prepared by catalytic decomposition of acetylene in a fluidized bed reactor. *J. Catal.* **2003**, *215* (2), 305–316.

(110) Schaper, A. K.; Hou, H.; Greiner, A.; Philipp, F. The role of iron carbide in multiwalled carbon nanotube growth. *J. Catal.* **2004**, *222* (1), 250–254.

(111) Perez-Cabero, M.; Romeo, E.; Royo, C.; Monzon, A.; Guerrero-Ruiz, A.; Rodriguez-Ramos, I. Growing mechanism of CNTs: a kinetic approach. *J. Catal.* **2004**, *224* (1), 197–205.

(112) Nishimura, K.; Okazaki, N.; Pan, L.; Nakayama, Y. In situ study of iron catalysts for carbon nanotube growth using X-ray diffraction analysis. *Jpn. J. Appl. Phys.* **2004**, *43*, L471–L474.

(113) Yoshida, H.; Takeda, S.; Uchiyama, T.; Kohno, H.; Homma, Y. Atomic-scale in-situ observation of carbon nanotube growth from solid state iron carbide nanoparticles. *Nano Lett.* **2008**, *8* (7), 2082–2086.

(114) Philippe, R.; Caussat, B.; Falqui, A.; Kihn, Y.; Kalck, P.; Bordère, S.; Plee, D.; Gaillard, P.; Bernard, D.; Serp, P. An original growth mode of MWCNTs on alumina supported iron catalysts. *J. Catal.* **2009**, *263* (2), 345–358.

(115) Sharma, R.; Moore, E.; Rez, P.; Treacy, M. M. J. Site-specific fabrication of Fe particles for carbon nanotube growth. *Nano Lett.* **2009**, *9* (2), 689–694.

(116) He, Z.; Maurice, J.-L.; Gohier, A.; Lee, C. S.; Pribat, D.; Cojocaru, C. S. Iron catalysts for the growth of carbon nanofibers: Fe, Fe₃C or Both? *Chem. Mater.* **2011**, *23* (24), 5379–5387.

(117) Wirth, C. T.; Bayer, B. C.; Gamalski, A. D.; Esconjauregui, S.; Weatherup, R. S.; Ducati, C.; Baetz, C.; Robertson, J.; Hofmann, S. The phase of iron catalyst nanoparticles during carbon nanotube growth. *Chem. Mater.* **2012**, *24* (24), 4633–4640.

(118) Reddy Enakonda, L.; Zhou, L.; Saih, Y.; Ould-Chikh, S.; Lopatin, S.; Gary, D.; Del-Gallo, P.; Basset, J.-M. Methane-induced activation mechanism of fused ferric oxide–alumina catalysts during methane decomposition. *ChemSusChem* **2016**, *9* (15), 1911–1915.

(119) Zhou, L.; Enakonda, L. R.; Harb, M.; Saih, Y.; Aguilar-Tapia, A.; Ould-Chikh, S.; Hazemann, J.-L.; Li, J.; Wei, N.; Gary, D.; Del-Gallo, P.; Basset, J.-M. Fe catalysts for methane decomposition to produce hydrogen and carbon nano materials. *Appl. Catal., B* **2017**, *208*, 44–59.

(120) Hofmann, S.; Blume, R.; Wirth, C. T.; Cantoro, M.; Sharma, R.; Ducati, C.; Hävecker, M.; Zafeiratos, S.; Schnoerch, P.; Oestereich, A.; Teschner, D.; Albrecht, M.; Knop-Gericke, A.; Schlögl, R.; Robertson, J. State of transition metal catalysts during carbon nanotube growth. *J. Phys. Chem. C* **2009**, *113* (5), 1648–1656.

(121) Cooper, B. J.; Trimm, D. L. Carbon deposition from propylene on polycrystalline and single crystal iron. *J. Catal.* **1980**, *62* (1), 35–43.

(122) Amin, A. M.; Croiset, E.; Epling, W. Review of methane catalytic cracking for hydrogen production. *Int. J. Hydrogen Energy* **2011**, *36* (4), 2904–2935.

(123) Avdeeva, L. B.; Reshetenko, T. V.; Ismagilov, Z. R.; Likholobov, V. A. Iron-containing catalysts of methane decomposition: accumulation of filamentous carbon. *Appl. Catal., A* **2002**, *228* (1–2), 53–63.

(124) Bayat, N.; Rezaei, M.; Meshkani, F. CO_x-free hydrogen and carbon nanofibers production by methane decomposition over nickel-alumina catalysts. *Korean J. Chem. Eng.* **2016**, *33* (2), 490–499.

(125) Bayat, N.; Rezaei, M.; Meshkani, F. Hydrogen and carbon nanofibers synthesis by methane decomposition over Ni-Pd/Al₂O₃ catalyst. *Int. J. Hydrogen Energy* **2016**, *41* (12), 5494–5503.

(126) Fakeeha, A. H.; Ibrahim, A. A.; Khan, W. U.; Seshan, K.; Al-Otaibi, R. L.; Al-Fatesh, A. S. Hydrogen production via catalytic methane decomposition over alumina supported iron catalyst. *Arabian J. Chem.* **2018**, *11* (3), 405–414.

(127) Rastegarpanah, A.; Rezaei, M.; Meshkani, F.; Zhang, K. F.; Zhao, X. T.; Pei, W. B.; Liu, Y. X.; Deng, J. G.; Arandiyani, H.; Dai, H. X. Mesoporous Ni/MeO_x (Me = Al, Mg, Ti, and Si): Highly efficient catalysts in the decomposition of methane for hydrogen production. *Appl. Surf. Sci.* **2019**, *478*, 581–593.

(128) Torres, D.; Pinilla, J. L.; Suelves, I. Co-, Cu- and Fe-doped Ni/Al₂O₃ catalysts for the catalytic decomposition of methane into hydrogen and carbon nanofibers. *Catalysts* **2018**, *8* (8), 1–15.

(129) Serrano, D. P.; Botas, J. A.; Pizarro, P.; Gómez, G. Kinetic and autocatalytic effects during the hydrogen production by methane decomposition over carbonaceous catalysts. *Int. J. Hydrogen Energy* **2013**, *38* (14), 5671–5683.

(130) Bayat, N.; Rezaei, M.; Meshkani, F. Methane decomposition over Ni-Fe/Al₂O₃ catalysts for production of CO_x-free hydrogen and carbon nanofiber. *Int. J. Hydrogen Energy* **2016**, *41* (3), 1574–1584.

(131) Bayat, N.; Meshkani, F.; Rezaei, M. Thermocatalytic decomposition of methane to CO_x-free hydrogen and carbon over Ni-Fe-Cu/Al₂O₃ catalysts. *Int. J. Hydrogen Energy* **2016**, *41* (30), 13039–13049.

(132) Wang, D.; Zhang, J.; Sun, J. B.; Gao, W. M.; Cui, Y. B. Effect of metal additives on the catalytic performance of Ni/Al₂O₃ catalyst in thermocatalytic decomposition of methane. *Int. J. Hydrogen Energy* **2019**, *44* (14), 7205–7215.

(133) Silva, R. R. C. M.; Oliveira, H. A.; Guarino, A. C. P. F.; Toledo, B. B.; Moura, M. B. T.; Oliveira, B. T. M.; Passos, F. B. Effect of support on methane decomposition for hydrogen production over cobalt catalysts. *Int. J. Hydrogen Energy* **2016**, *41* (16), 6763–6772.

(134) Pudukudy, M.; Yaakob, Z. Methane decomposition over Ni, Co and Fe based monometallic catalysts supported on sol gel derived SiO₂ microflakes. *Chem. Eng. J.* **2015**, *262*, 1009–1021.

- (135) Ibrahim, A. A.; Al-Fatesh, A. S.; Khan, W. U.; Soliman, M. A.; Al-Otaibi, R. L.; Fakeeha, A. H. Thermo-catalytic methane decomposition: A review of state of the art of catalysts. *J. Chem. Soc. Pak.* **2015**, *37* (6), 1269–1297.
- (136) Al-Fatesh, A. S.; Amin, A.; Ibrahim, A. A.; Khan, W. U.; Soliman, M. A.; Al-Otaibi, R. L.; Fakeeha, A. H. Effect of Ce and Co addition to Fe/Al₂O₃ for catalytic methane decomposition. *Catalysts* **2016**, *6* (3), 15.
- (137) Al-Fatesh, A. S.; Fakeeha, A. H.; Khan, W. U.; Ibrahim, A. A.; He, S. B.; Seshan, K. Production of hydrogen by catalytic methane decomposition over alumina supported mono-, bi- and tri-metallic catalysts. *Int. J. Hydrogen Energy* **2016**, *41* (48), 22932–22940.
- (138) Al-Fatesh, A. S.; Barama, S.; Ibrahim, A. A.; Barama, A.; Khan, W. U.; Fakeeha, A. Study of methane decomposition on Fe/MgO-based catalyst modified by Ni, Co, and Mn additives. *Chem. Eng. Commun.* **2017**, *204* (7), 739–749.
- (139) Pudukudy, M.; Yaakob, Z.; Takriff, M. S. Methane decomposition into CO_x free hydrogen and multiwalled carbon nanotubes over ceria, zirconia and lanthana supported nickel catalysts prepared via a facile solid state citrate fusion method. *Energy Convers. Manage.* **2016**, *126*, 302–315.
- (140) Awadallah, A. E.; Solyman, S. M.; Aboul-Enein, A. A.; Ahmed, H. A.; Aboul-Gheit, N. A. K.; Hassan, S. A. Effect of combining Al, Mg, Ce or La oxides to extracted rice husk nanosilica on the catalytic performance of NiO during CO_x-free hydrogen production via methane decomposition. *Int. J. Hydrogen Energy* **2017**, *42* (15), 9858–9872.
- (141) Pudukudy, M.; Yaakob, Z.; Jia, Q. M.; Takriff, M. S. Catalytic decomposition of methane over rare earth metal (Ce and La) oxides supported iron catalysts. *Appl. Surf. Sci.* **2019**, *467*, 236–248.
- (142) Ermakova, M. A.; Ermakov, D. Y. Ni/SiO₂ and Fe/SiO₂ catalysts for production of hydrogen and filamentous carbon via methane decomposition. *Catal. Today* **2002**, *77* (3), 225–235.
- (143) Ouyang, M. Z.; Boldrin, P.; Maher, R. C.; Chen, X. L.; Liu, X. H.; Cohen, L. F.; Brandon, N. P. A mechanistic study of the interactions between methane and nickel supported on doped ceria. *Appl. Catal., B* **2019**, *248*, 332–340.
- (144) Guil-López, R.; Botas, J. A.; Fierro, J. L. G.; Serrano, D. P. Comparison of metal and carbon catalysts for hydrogen production by methane decomposition. *Appl. Catal., A* **2011**, *396* (1–2), 40–51.
- (145) Li, J. M.; Zhao, L. J.; He, J. C.; Dong, L.; Xiong, L. P.; Du, Y.; Yang, Y.; Wang, H. Y.; Peng, S. M. Methane decomposition over high-loaded Ni-Cu-SiO₂ catalysts. *Fusion Eng. Des.* **2016**, *113*, 279–287.
- (146) Berndt, F. M.; Perez-Lopez, O. W. Catalytic decomposition of methane over Ni/SiO₂: influence of Cu addition. *React. Kinet., Mech. Catal.* **2017**, *120* (1), 181–193.
- (147) Al-Fatesh, A. S.; Fakeeha, A. H.; Ibrahim, A. A.; Khan, W. U.; Atia, H.; Eckelt, R.; Seshan, K.; Chowdhury, B. Decomposition of methane over alumina supported Fe and Ni-Fe bimetallic catalyst: Effect of preparation procedure and calcination temperature. *J. Saudi Chem. Soc.* **2018**, *22* (2), 239–247.
- (148) Rastegarpanah, A.; Rezaei, M.; Meshkani, F.; Zhang, K. F.; Zhao, X. T.; Pei, W. B.; Liu, Y. X.; Deng, J. G.; Arandiyani, H.; Dai, H. X. Influence of group VIB metals on activity of the Ni/MgO catalysts for methane decomposition. *Appl. Catal., B* **2019**, *248*, 515–525.
- (149) Pudukudy, M.; Yaakob, Z.; Mazuki, M. Z.; Takriff, M. S.; Jahaya, S. S. One-pot sol-gel synthesis of MgO nanoparticles supported nickel and iron catalysts for undiluted methane decomposition into CO_x free hydrogen and nanocarbon. *Appl. Catal., B* **2017**, *218*, 298–316.
- (150) Takenaka, S.; Ogihara, H.; Yamanaka, I.; Otsuka, K. Decomposition of methane over supported-Ni catalysts: effects of the supports on the catalytic lifetime. *Appl. Catal., A* **2001**, *217* (1–2), 101–110.
- (151) Takenaka, S.; Shigeta, Y.; Tanabe, E.; Otsuka, K. Methane decomposition into hydrogen and carbon nanofibers over supported Pd-Ni catalysts. *J. Catal.* **2003**, *220* (2), 468–477.
- (152) Garcia-Sancho, C.; Guil-López, R.; Sebastian-Lopez, A.; Navarro, R. M.; Fierro, J. L. G. Hydrogen production by methane decomposition: A comparative study of supported and bulk ex-hydrocalcite mixed oxide catalysts with Ni, Mg and Al. *Int. J. Hydrogen Energy* **2018**, *43* (20), 9607–9621.
- (153) Awadallah, A. E.; Mostafa, M. S.; Aboul-Enein, A. A.; Hanafi, S. A. Hydrogen production via methane decomposition over Al₂O₃-TiO₂ binary oxides supported Ni catalysts: Effect of Ti content on the catalytic efficiency. *Fuel* **2014**, *129*, 68–77.
- (154) Ahmed, W.; Awadallah, A. E.; Aboul-Enein, A. A. Ni/CeO₂-Al₂O₃ catalysts for methane thermo-catalytic decomposition to CO_x-free H₂ production. *Int. J. Hydrogen Energy* **2016**, *41* (41), 18484–18493.
- (155) Li, Y.; Li, D.; Wang, G. Methane decomposition to CO_x-free hydrogen and nano-carbon material on group 8–10 base metal catalysts: A review. *Catal. Today* **2011**, *162* (1), 1–48.
- (156) Naresh, G.; Kumar, V. V.; Anjaneyulu, C.; Tardio, J.; Bhargava, S. K.; Patel, J.; Venugopal, A. Nano size H beta zeolite as an effective support for Ni and Ni-Cu for CO_x free hydrogen production by catalytic decomposition of methane. *Int. J. Hydrogen Energy* **2016**, *41* (44), 19855–19862.
- (157) Shen, Y.; Lua, A. C. Synthesis of Ni and Ni-Cu supported on carbon nanotubes for hydrogen and carbon production by catalytic decomposition of methane. *Appl. Catal., B* **2015**, *164*, 61–69.
- (158) Torres, D.; Pinilla, J. L.; Suelves, I. Screening of Ni-Cu bimetallic catalysts for hydrogen and carbon nanofilaments production via catalytic decomposition of methane. *Appl. Catal., A* **2018**, *559*, 10–19.
- (159) Rai, R. K.; Gupta, K.; Tyagi, D.; Mahata, A.; Behrens, S.; Yang, X.; Xu, Q.; Pathak, B.; Singh, S. K. Access to highly active Ni-Pd bimetallic nanoparticle catalysts for C-C coupling reactions. *Catal. Sci. Technol.* **2016**, *6* (14), 5567–5579.
- (160) Huynh, T.-T.; Tsai, M.-C.; Pan, C.-J.; Su, W.-N.; Chan, T.-S.; Lee, J.-F.; Hwang, B.-J. Synergetic electrocatalytic activities towards hydrogen peroxide: Understanding the ordered structure of PdNi bimetallic nanocatalysts. *Electrochem. Commun.* **2019**, *101*, 93–98.
- (161) Miao, C.; Zhou, G.; Chen, S.; Xie, H.; Zhang, X. Synergistic effects between Cu and Ni species in NiCu/γ-Al₂O₃ catalysts for hydrodeoxygenation of methyl laurate. *Renewable Energy* **2020**, *153*, 1439–1454.
- (162) Wang, H. Y.; Lua, A. C. Methane decomposition using Ni-Cu alloy nano-particle catalysts and catalyst deactivation studies. *Chem. Eng. J.* **2015**, *262*, 1077–1089.
- (163) Echevoyen, Y.; Suelves, I.; Lázaro, M. J.; Moliner, R.; Palacios, J. M. Hydrogen production by thermocatalytic decomposition of methane over Ni-Al and Ni-Cu-Al catalysts: Effect of calcination temperature. *J. Power Sources* **2007**, *169* (1), 150–157.
- (164) Saraswat, S. K.; Pant, K. K. Ni-Cu-Zn/MCM-22 catalysts for simultaneous production of hydrogen and multiwall carbon nanotubes via thermo-catalytic decomposition of methane. *Int. J. Hydrogen Energy* **2011**, *36* (21), 13352–13360.
- (165) Pudukudy, M.; Yaakob, Z.; Akmal, Z. S. Direct decomposition of methane over Pd promoted Ni/SBA-15 catalysts. *Appl. Surf. Sci.* **2015**, *353*, 127–136.
- (166) Pudukudy, M.; Yaakob, Z.; Takriff, M. S. Methane decomposition over Pd promoted Ni/MgAl₂O₄ catalysts for the production of CO_x free hydrogen and multiwalled carbon nanotubes. *Appl. Surf. Sci.* **2015**, *356*, 1320–1326.
- (167) Rastegarpanah, A.; Meshkani, F.; Rezaei, M. Thermocatalytic decomposition of methane over mesoporous nanocrystalline promoted Ni/MgO-Al₂O₃ catalysts. *Int. J. Hydrogen Energy* **2017**, *42* (26), 16476–16488.
- (168) Ashok, J.; Reddy, P. S.; Raju, G.; Subrahmanyam, M.; Venugopal, A. Catalytic decomposition of methane to hydrogen and carbon nanofibers over Ni-Cu-SiO₂ catalysts. *Energy Fuels* **2009**, *23* (1), 5–13.
- (169) Wang, J. F.; Jin, L. J.; Li, Y.; Hu, H. Q. Preparation of Fe-doped carbon catalyst for methane decomposition to hydrogen. *Ind. Eng. Chem. Res.* **2017**, *56* (39), 11021–11027.
- (170) Ibrahim, A. A.; Fakeeha, A. H.; Al-Fatesh, A. S.; Abasaheed, A. E.; Khan, W. U. Methane decomposition over iron catalyst for

hydrogen production. *Int. J. Hydrogen Energy* **2015**, *40* (24), 7593–7600.

(171) Cunha, A. F.; Orfão, J. J. M.; Figueiredo, J. L. Methane decomposition on Fe-Cu Raney-type catalysts. *Fuel Process. Technol.* **2009**, *90* (10), 1234–1240.

(172) Al-Fatesh, A. S.; Abu-Dahrieh, J.; Ibrahim, A. A.; Fakeeha, A. H.; Khan, W. U. Coproduction of hydrogen and carbon filaments from methane decomposition over Fe/La₂O₃ Catalysts. *J. Chem. Soc. Pak.* **2016**, *38* (6), 1104–1111.

(173) Al-Fatesh, A. S.; Fakeeha, A. H.; Ibrahim, A. A.; Khan, W. U.; Atia, H.; Eckelt, R.; Chowdhury, B. Iron oxide supported on Al₂O₃ catalyst for methane decomposition reaction: Effect of MgO additive and calcination Temperature. *J. Chin. Chem. Soc.* **2016**, *63* (2), 205–212.

(174) Zhou, L.; Enakonda, L. R.; Saih, Y.; Loptain, S.; Gary, D.; Del-Gallo, P.; Basset, J.-M. Catalytic methane decomposition over Fe-Al₂O₃. *ChemSusChem* **2016**, *9* (11), 1243–1248.

(175) Zhou, L.; Enakonda, L. R.; Li, S.; Gary, D.; Del-Gallo, P.; Mennemann, C.; Basset, J.-M. Iron ore catalysts for methane decomposition to make CO_x free hydrogen and carbon nano material. *J. Taiwan Inst. Chem. Eng.* **2018**, *87*, 54–63.

(176) Sánchez-Bastardo, N.; Schlögl, R.; Ruland, H. Methane pyrolysis for CO₂-free H₂ production: A green process to overcome renewable energies unsteadiness. *Chem. Ing. Tech.* **2020**, *92* (10), 1596–1609.

(177) Shah, N.; Pattanaik, S.; Huggins, F. E.; Panjala, D.; Huffman, G. P. XAFS and Mössbauer spectroscopy characterization of supported binary catalysts for nonoxidative dehydrogenation of methane. *Fuel Process. Technol.* **2003**, *83* (1), 163–173.

(178) Punnoose, A.; Shah, N.; Huffman, G. P.; Seehra, M. S. X-ray diffraction and electron magnetic resonance studies of M/Fe/Al₂O₃ (M = Ni, Mo and Pd) catalysts for CH₄ to H₂ conversion. *Fuel Process. Technol.* **2003**, *83* (1), 263–273.

(179) Awadallah, A. E.; Aboul-Enein, A. A.; Azab, M. A.; Abdel-Monem, Y. K. Influence of Mo or Cu doping in Fe/MgO catalyst for synthesis of single-walled carbon nanotubes by catalytic chemical vapor deposition of methane. *Fullerenes, Nanotubes, Carbon Nanostruct.* **2017**, *25* (4), 256–264.

(180) Fakeeha, A. H.; Al-Fatesh, A. S.; Chowdhury, B.; Ibrahim, A. A.; Khan, W. U.; Hassan, S.; Sasudeen, K.; Abasaeed, A. E. Bi-metallic catalysts of mesoporous Al₂O₃ supported on Fe, Ni and Mn for methane decomposition: Effect of activation temperature. *Chin. J. Chem. Eng.* **2018**, *26* (9), 1904–1911.

(181) Pinilla, J. L.; Utrilla, R.; Karn, R. K.; Suelves, I.; Lázaro, M. J.; Moliner, R.; García, A. B.; Rouzaud, J. N. High temperature iron-based catalysts for hydrogen and nanostructured carbon production by methane decomposition. *Int. J. Hydrogen Energy* **2011**, *36* (13), 7832–7843.

(182) Ramasubramanian, V.; Ramsurn, H.; Price, G. L. Hydrogen production by catalytic decomposition of methane over Fe based bi-metallic catalysts supported on CeO₂-ZrO₂. *Int. J. Hydrogen Energy* **2020**, *45* (21), 12026–12036.

(183) Calafat, A.; Sanchez, N. Production of carbon nanotubes through combination of catalyst reduction and methane decomposition over Fe-Ni/ZrO₂ catalysts prepared by the citrate method. *Appl. Catal., A* **2016**, *528*, 14–23.

(184) Tang, L.; Yamaguchi, D.; Burke, N.; Trimm, D.; Chiang, K. Methane decomposition over ceria modified iron catalysts. *Catal. Commun.* **2010**, *11* (15), 1215–1219.

(185) Barreiro, A.; Hampel, S.; Rümmeli, M. H.; Kramberger, C.; Grüneis, A.; Biedermann, K.; Leonhardt, A.; Gemming, T.; Büchner, B.; Bachtold, A.; Pichler, T. Thermal decomposition of ferrocene as a method for production of single-walled carbon nanotubes without additional carbon sources. *J. Phys. Chem. B* **2006**, *110* (42), 20973–20977.

(186) Huang, G.; Weng, J. Syntheses of carbon nanomaterials by ferrocene. *Curr. Org. Chem.* **2011**, *15* (21), 3653–3666.

(187) Rao, C. N. R.; Sen, R.; Satishkumar, B. C.; Govindaraj, A. Large aligned-nanotube bundles from ferrocene pyrolysis. *Chem. Commun.* **1998**, *15*, 1525–1526.

(188) Satishkumar, B. C.; Govindaraj, A.; Rao, C. N. R. Bundles of aligned carbon nanotubes obtained by the pyrolysis of ferrocene-hydrocarbon mixtures: role of the metal nanoparticles produced in situ. *Chem. Phys. Lett.* **1999**, *307* (3), 158–162.

(189) Rao, C. N. R.; Govindaraj, A. Carbon nanotubes from organometallic precursors. *Acc. Chem. Res.* **2002**, *35* (12), 998–1007.

(190) Leonhardt, A.; Ritschel, M.; Elefant, D.; Mattern, N.; Biedermann, K.; Hampel, S.; Müller, C.; Gemming, T.; Büchner, B. Enhanced magnetism in Fe-filled carbon nanotubes produced by pyrolysis of ferrocene. *J. Appl. Phys.* **2005**, *98* (7), 074315.

(191) Zhang, T. J.; Amiridis, M. D. Hydrogen production via the direct cracking of methane over silica-supported nickel catalysts. *Appl. Catal., A* **1998**, *167* (2), 161–172.

(192) Villacampa, J. I.; Royo, C.; Romeo, E.; Montoya, J. A.; Del Angel, P.; Monzón, A. Catalytic decomposition of methane over Ni-Al₂O₃ coprecipitated catalysts: Reaction and regeneration studies. *Appl. Catal., A* **2003**, *252* (2), 363–383.

(193) Otsuka, K.; Takenaka, S.; Ohtsuki, H. Production of pure hydrogen by cyclic decomposition of methane and oxidative elimination of carbon nanofibers on supported-Ni-based catalysts. *Appl. Catal., A* **2004**, *273* (1), 113–124.

(194) Rahman, M. S.; Croiset, E.; Hudgins, R. R. Catalytic decomposition of methane for hydrogen production. *Top. Catal.* **2006**, *37* (2), 137–145.

(195) Ammendola, P.; Chirone, R.; Ruoppolo, G.; Russo, G. Regeneration strategies of deactivated catalysts for thermo-catalytic decomposition process in a fluidized bed reactor. *Combust. Sci. Technol.* **2008**, *180* (5), 869–882.

(196) Li, J.; Smith, K. J. Methane decomposition and catalyst regeneration in a cyclic mode over supported Co and Ni catalysts. *Appl. Catal., A* **2008**, *349* (1), 116–124.

(197) Saraswat, S. K.; Pant, K. K. Synthesis of hydrogen and carbon nanotubes over copper promoted Ni/SiO₂ catalyst by thermocatalytic decomposition of methane. *J. Nat. Gas Sci. Eng.* **2013**, *13*, 52–59.

(198) Aiello, R.; Fiscus, J. E.; zur Loye, H.-C.; Amiridis, M. D. Hydrogen production via the direct cracking of methane over Ni/SiO₂ catalyst deactivation and regeneration. *Appl. Catal., A* **2000**, *192* (2), 227–234.

(199) Choudhary, V. R.; Banerjee, S.; Rajput, A. M. Continuous production of H₂ at low temperature from methane decomposition over Ni-containing catalyst followed by gasification by steam of the carbon on the catalyst in two parallel reactors operated in cyclic manner. *J. Catal.* **2001**, *198* (1), 136–141.

(200) Takenaka, S.; Tomikubo, Y.; Kato, E.; Otsuka, K. Sequential production of H₂ and CO over supported Ni catalysts. *Fuel* **2004**, *83* (1), 47–57.

(201) Al-Hassani, A. A.; Abbas, H. F.; Daud, W. M. A. W. Production of CO_x-free hydrogen by the thermal decomposition of methane over activated carbon: Catalyst deactivation. *Int. J. Hydrogen Energy* **2014**, *39* (27), 14783–14791.

(202) Muradov, N. Z. CO₂-free production of hydrogen by catalytic pyrolysis of hydrocarbon fuel. *Energy Fuels* **1998**, *12* (1), 41–48.

(203) Muradov, N. Catalysis of methane decomposition over elemental carbon. *Catal. Commun.* **2001**, *2* (3–4), 89–94.

(204) Muradov, N. Hydrogen via methane decomposition: An application for decarbonization of fossil fuels. *Int. J. Hydrogen Energy* **2001**, *26* (11), 1165–1175.

(205) Ryu, B. H.; Lee, S. Y.; Lee, D. H.; Han, G. Y.; Lee, T.-J.; Yoon, K. J. Catalytic characteristics of various rubber-reinforcing carbon blacks in decomposition of methane for hydrogen production. *Catal. Today* **2007**, *123* (1–4), 303–309.

(206) Suelves, I.; Lázaro, M. J.; Moliner, R.; Pinilla, J. L.; Cubero, H. Hydrogen production by methane decarbonization: Carbonaceous catalysts. *Int. J. Hydrogen Energy* **2007**, *32* (15), 3320–3326.

(207) Serrano, D. P.; Botas, J. A.; Pizarro, P.; Guil-López, R.; Gómez, G. Ordered mesoporous carbons as highly active catalysts for

hydrogen production by CH₄ decomposition. *Chem. Commun.* **2008**, 48, 6585–6587.

(208) Suelves, I.; Pinilla, J. L.; Lázaro, M. J.; Moliner, R. Carbonaceous materials as catalysts for decomposition of methane. *Chem. Eng. J.* **2008**, *140* (1–3), 432–438.

(209) Botas, J. A.; Serrano, D. P.; Guil-López, R.; Pizarro, P.; Gómez, G. Methane catalytic decomposition over ordered mesoporous carbons: A promising route for hydrogen production. *Int. J. Hydrogen Energy* **2010**, *35* (18), 9788–9794.

(210) Ghani, S. A.; Al Saraj, M. A. A.; Razaq, G. H. A. Catalytic production of CO_x free hydrogen by methane decomposition over activated carbons. *Energy Sources, Part A* **2015**, *37* (3), 326–333.

(211) Nishii, H.; Miyamoto, D.; Umeda, Y.; Hamaguchi, H.; Suzuki, M.; Tanimoto, T.; Harigai, T.; Takikawa, H.; Suda, Y. Catalytic activity of several carbons with different structures for methane decomposition and by-produced carbons. *Appl. Surf. Sci.* **2019**, *473*, 291–297.

(212) Serrano, D. P.; Botas, J. A.; Guil-López, R. H₂ production from methane pyrolysis over commercial carbon catalysts: Kinetic and deactivation study. *Int. J. Hydrogen Energy* **2009**, *34* (10), 4488–4494.

(213) Wang, H. Y.; Lua, A. C. Hydrogen production by thermocatalytic methane decomposition. *Heat Transfer Eng.* **2013**, *34* (11–12), 896–903.

(214) Krzyżyński, S.; Kozłowski, M. Activated carbons as catalysts for hydrogen production via methane decomposition. *Int. J. Hydrogen Energy* **2008**, *33* (21), 6172–6177.

(215) Muradov, N. *Thermocatalytic CO₂-free production of hydrogen from hydrocarbon fuels Proceedings of the 2000 Hydrogen Program Review*; NREL/CP-570–28890, National Renewable Energy Laboratory: Golden CO, 2000.

(216) Bai, Z. Q.; Chen, H. K.; Li, W.; Li, B. Q. Hydrogen production by methane decomposition over coal char. *Int. J. Hydrogen Energy* **2006**, *31* (7), 899–905.

(217) Moliner, R.; Suelves, I.; Lázaro, M. J.; Moreno, O. Thermocatalytic decomposition of methane over activated carbons: influence of textural properties and surface chemistry. *Int. J. Hydrogen Energy* **2005**, *30* (3), 293–300.

(218) Pinilla, J. L.; Suelves, I.; Utrilla, R.; Gálvez, M. E.; Lázaro, M. J.; Moliner, R. Hydrogen production by thermo-catalytic decomposition of methane: Regeneration of active carbons using CO₂. *J. Power Sources* **2007**, *169* (1), 103–109.

(219) Pinilla, J. L.; Suelves, I.; Lázaro, M. J.; Moliner, R. Kinetic study of the thermal decomposition of methane using carbonaceous catalysts. *Chem. Eng. J.* **2008**, *138* (1), 301–306.

(220) Bai, Z. Q.; Chen, H.; Li, B. Q.; Li, W. Catalytic decomposition of methane over activated carbon. *J. Anal. Appl. Pyrolysis* **2005**, *73* (2), 335–341.

(221) Lázaro, M. J.; Pinilla, J. L.; Suelves, I.; Moliner, R. Study of the deactivation mechanism of carbon blacks used in methane decomposition. *Int. J. Hydrogen Energy* **2008**, *33* (15), 4104–4111.

(222) Sun, Z.-Q.; Wu, J.-H.; Haghghi, M.; Bromly, J.; Ng, E.; Wee, H. L.; Wang, Y.; Zhang, D.-K. Methane cracking over a bituminous coal char. *Energy Fuels* **2007**, *21* (3), 1601–1605.

(223) Abbas, H. F.; Daud, W. M. A. W. Thermocatalytic decomposition of methane for hydrogen production using activated carbon catalyst: Regeneration and characterization studies. *Int. J. Hydrogen Energy* **2009**, *34* (19), 8034–8045.

(224) Abbas, H. F.; Daud, W. M. A. W. An experimental investigation into the CO₂ gasification of deactivated activated-carbon catalyst used for methane decomposition to produce hydrogen. *Int. J. Hydrogen Energy* **2010**, *35* (1), 141–150.

(225) Muradov, N.; Chen, Z.; Smith, F. Fossil hydrogen with reduced CO₂ emission: Modeling thermocatalytic decomposition of methane in a fluidized bed of carbon particles. *Int. J. Hydrogen Energy* **2005**, *30* (10), 1149–1158.

(226) Dufour, A.; Celzard, A.; Fierro, V.; Broust, F.; Courson, C.; Zoulalian, A.; Rouzaud, J. N. Catalytic conversion of methane over a biomass char for hydrogen production: deactivation and regeneration by steam gasification. *Appl. Catal., A* **2015**, *490*, 170–180.

(227) Malaika, A.; Kozłowski, M. Influence of ethylene on carbon-catalysed decomposition of methane. *Int. J. Hydrogen Energy* **2009**, *34* (6), 2600–2605.

(228) Malaika, A.; Kozłowski, M. Hydrogen production by propylene-assisted decomposition of methane over activated carbon catalysts. *Int. J. Hydrogen Energy* **2010**, *35* (19), 10302–10310.

(229) Malaika, A.; Krzyzyska, B.; Kozłowski, M. Catalytic decomposition of methane in the presence of in situ obtained ethylene as a method of hydrogen production. *Int. J. Hydrogen Energy* **2010**, *35* (14), 7470–7475.

(230) Adamska, A.; Malaika, A.; Kozłowski, M. Carbon-catalyzed decomposition of methane in the presence of carbon dioxide. *Energy Fuels* **2010**, *24* (6), 3307–3312.

(231) Rechnia, P.; Malaika, A.; Krzyzyska, B.; Kozłowski, M. Decomposition of methane in the presence of ethanol over activated carbon catalyst. *Int. J. Hydrogen Energy* **2012**, *37* (19), 14178–14186.

(232) Rechnia, P.; Malaika, A.; Najder-Kozdrowska, L.; Kozłowski, M. The effect of ethanol on carbon-catalysed decomposition of methane. *Int. J. Hydrogen Energy* **2012**, *37* (9), 7512–7520.

(233) Ogihara, H.; Tajima, H.; Kurokawa, H. Pyrolysis of mixtures of methane and ethane: activation of methane with the aid of radicals generated from ethane. *React. Chem. Eng.* **2020**, *5* (1), 145–153.

(234) Bai, Z. Q.; Chen, H. K.; Li, B. Q.; Li, W. Methane decomposition over Ni loaded activated carbon for hydrogen production and the formation of filamentous carbon. *Int. J. Hydrogen Energy* **2007**, *32* (1), 32–37.

(235) Pinilla, J. L.; Suelves, I.; Lázaro, M. J.; Moliner, R.; Palacios, J. M. Parametric study of the decomposition of methane using a NiCu/Al₂O₃ catalyst in a fluidized bed reactor. *Int. J. Hydrogen Energy* **2010**, *35* (18), 9801–9809.

(236) Szymańska, M.; Malaika, A.; Rechnia, P.; Miklaszewska, A.; Kozłowski, M. Metal/activated carbon systems as catalysts of methane decomposition reaction. *Catal. Today* **2015**, *249*, 94–102.

(237) Nasir Uddin, M.; Wan Daud, W.M.A.; Abbas, H. F. Co-production of hydrogen and carbon nanofibers from methane decomposition over zeolite Y supported Ni catalysts. *Energy Convers. Manage.* **2015**, *90*, 218–229.

(238) Pudukudy, M.; Yaakob, Z.; Takriff, M. S. Methane decomposition over unsupported mesoporous nickel ferrites: effect of reaction temperature on the catalytic activity and properties of the produced nanocarbon. *RSC Adv.* **2016**, *6* (72), 68081–68091.

(239) Salipira, K.; Coville, N. J.; Scurrell, M. S. Carbon produced by the catalytic decomposition of methane on nickel: Carbon yields and carbon structure as a function of catalyst properties. *J. Nat. Gas Sci. Eng.* **2016**, *32*, 501–511.

(240) Ashik, U.P.M.; Wan Daud, W.M.A.; Abbas, H. F. Methane decomposition kinetics and reaction rate over Ni/SiO₂ nanocatalyst produced through co-precipitation cum modified Stober method. *Int. J. Hydrogen Energy* **2017**, *42* (2), 938–952.

(241) Urdiana, G.; Valdez, R.; Lastra, G.; Valenzuela, M. Á.; Olivas, A. Production of hydrogen and carbon nanomaterials using transition metal catalysts through methane decomposition. *Mater. Lett.* **2018**, *217*, 9–12.

(242) Abbas, H. F.; Daud, W. M. A. W. Deactivation of palm shell-based activated carbon catalyst used for hydrogen production by thermocatalytic decomposition of methane. *Int. J. Hydrogen Energy* **2009**, *34* (15), 6231–6241.

(243) Abbas, H. F.; Baker, I. F. Thermocatalytic decomposition of methane using activated carbon: Studying the influence of process parameters using factorial design. *Int. J. Hydrogen Energy* **2011**, *36* (15), 8985–8993.

(244) Shilapuram, V.; Ozalp, N.; Oschatz, M.; Borchardt, L.; Kaskel, S. Hydrogen production from catalytic decomposition of methane over ordered mesoporous carbons (CMK-3) and carbide-derived carbon (DUT-19). *Carbon* **2014**, *67*, 377–389.

(245) Fakeeha, A. H.; Khan, W. U.; Al-Fatesh, A. S.; Abasaheed, A. E.; Naem, M. A. Production of hydrogen and carbon nanofibers from methane over Ni-Co-Al catalysts. *Int. J. Hydrogen Energy* **2015**, *40* (4), 1774–1781.

- (246) Pudukudy, M.; Yaakob, Z.; Kadier, A.; Takriff, M. S.; Hassan, N. S. M. One-pot sol-gel synthesis of Ni/TiO₂ catalysts for methane decomposition into CO_x free hydrogen and multiwalled carbon nanotubes. *Int. J. Hydrogen Energy* **2017**, *42* (26), 16495–16513.
- (247) Rastegarpanah, A.; Meshkani, F.; Rezaei, M. CO_x-free hydrogen and carbon nanofibers production by thermocatalytic decomposition of methane over mesoporous MgO·Al₂O₃ nanopowder-supported nickel catalysts. *Fuel Process. Technol.* **2017**, *167*, 250–262.
- (248) Tezel, E.; Figen, H. E.; Baykara, S. Z. Hydrogen production by methane decomposition using bimetallic Ni-Fe catalysts. *Int. J. Hydrogen Energy* **2019**, *44*, 9930–9940.
- (249) Zhang, W.; Ge, Q. J.; Xu, H. Y. Influences of reaction conditions on methane decomposition over non-supported Ni catalyst. *J. Nat. Gas Chem.* **2011**, *20* (4), 339–344.
- (250) Pinilla, J. L.; Suelves, I.; Lázaro, M. J.; Moliner, R. Influence on hydrogen production of the minor components of natural gas during its decomposition using carbonaceous catalysts. *J. Power Sources* **2009**, *192* (1), 100–106.
- (251) Fidalgo, B.; Muradov, N.; Menéndez, J. A. Effect of H₂S on carbon-catalyzed methane decomposition and CO₂ reforming reactions. *Int. J. Hydrogen Energy* **2012**, *37* (19), 14187–14194.
- (252) Munera Parra, A. A., Reactor design, modeling and optimization for the high-temperature methane pyrolysis and the reverse water-gas shift reaction. Ph.D, Thesis Fakultät Bio- und Chemieingenieurwesen der Technischen Universität: Dortmund, 2018.
- (253) Serban, M.; Lewis, M. A.; Marshall, C. L.; Doctor, R. D. Hydrogen production by direct contact pyrolysis of natural gas. *Energy Fuels* **2003**, *17* (3), 705–713.
- (254) Geißler, T.; Plevan, M.; Abánades, A.; Heinzl, A.; Mehravarán, K.; Rathnam, R. K.; Rubbia, C.; Salmieri, D.; Stoppel, L.; Stückrad, S.; Weisenburger, A.; Wenninger, H.; Wetzl, T. Experimental investigation and thermo-chemical modeling of methane pyrolysis in a liquid metal bubble column reactor with a packed bed. *Int. J. Hydrogen Energy* **2015**, *40* (41), 14134–14146.
- (255) Plevan, M.; Geißler, T.; Abánades, A.; Mehravarán, K.; Rathnam, R. K.; Rubbia, C.; Salmieri, D.; Stoppel, L.; Stückrad, S.; Wetzl, T. Thermal cracking of methane in a liquid metal bubble column reactor: Experiments and kinetic analysis. *Int. J. Hydrogen Energy* **2015**, *40* (25), 8020–8033.
- (256) Geißler, T.; Abánades, A.; Heinzl, A.; Mehravarán, K.; Müller, G.; Rathnam, R. K.; Rubbia, C.; Salmieri, D.; Stoppel, L.; Stückrad, S.; Weisenburger, A.; Wenninger, H.; Wetzl, T. Hydrogen production via methane pyrolysis in a liquid metal bubble column reactor with a packed bed. *Chem. Eng. J.* **2016**, *299*, 192–200.
- (257) Abánades, A.; Rathnam, R. K.; Geißler, T.; Heinzl, A.; Mehravarán, K.; Müller, G.; Plevan, M.; Rubbia, C.; Salmieri, D.; Stoppel, L.; Stückrad, S.; Weisenburger, A.; Wenninger, H.; Wetzl, T. Development of methane decarbonisation based on liquid metal technology for CO₂-free production of hydrogen. *Int. J. Hydrogen Energy* **2016**, *41* (19), 8159–8167.
- (258) Upham, D. C.; Agarwal, V.; Khechfe, A.; Snodgrass, Z. R.; Gordon, M. J.; Metiu, H.; McFarland, E. W. Catalytic molten metals for the direct conversion of methane to hydrogen and separable carbon. *Science* **2017**, *358* (6365), 917–920.
- (259) Munera Parra, A. A.; Agar, D. W. Molten metal capillary reactor for the high-temperature pyrolysis of methane. *Int. J. Hydrogen Energy* **2017**, *42* (19), 13641–13648.
- (260) Kang, D.; Rahimi, N.; Gordon, M. J.; Metiu, H.; McFarland, E. W. Catalytic methane pyrolysis in molten MnCl₂-KCl. *Appl. Catal., B* **2019**, *254*, 659–666.
- (261) Rahimi, N.; Kang, D.; Gelinas, J.; Menon, A.; Gordon, M. J.; Metiu, H.; McFarland, E. W. Solid carbon production and recovery from high temperature methane pyrolysis in bubble columns containing molten metals and molten salts. *Carbon* **2019**, *151*, 181–191.
- (262) Palmer, C.; Tarazkar, M.; Kristoffersen, H. H.; Gelinas, J.; Gordon, M. J.; McFarland, E. W.; Metiu, H. Methane pyrolysis with a molten Cu-Bi alloy catalyst. *ACS Catal.* **2019**, *9* (9), 8337–8345.
- (263) Leal Pérez, B. J.; Medrano Jiménez, J. A.; Bhardwaj, R.; Goetheer, E.; van Sint Annaland, M.; Gallucci, F. Methane pyrolysis in a molten gallium bubble column reactor for sustainable hydrogen production: Proof of concept & techno-economic assessment. *Int. J. Hydrogen Energy* **2021**, *46* (7), 4917–4935.
- (264) Yan, W.; Hoekman, S. K. Production of CO₂-free hydrogen from methane dissociation: A review. *Environ. Prog. Sustainable Energy* **2014**, *33* (1), 213–219.
- (265) Bode, A.; Anderlohr, C.; Bernnat, J.; Flick, D.; Glenk, F.; Klinger, D.; Kolios, G.; Scheiff, F.; Wechsung, A.; Hensmann, M.; Möhring, S.; Stubbe, G.; Lizandara, C.; Lange de Oliveira, A.; Schunk, S. A.; Göke, V.; Hunfeld, J.; Mihailowitsch, D.; Pleintinger, S.; Posselt, H.; Weikl, M. C.; Zander, H.-J.; Antweiler, N.; Büker, K.; Eckbauer, M.; Krüger, M.; Marek, P.; Rodermund, K.; Janhsen, U.; Mittelstädt, H.; Möllers, C.; Agar, D. W.; Munera-Parra, A. A. *Feste und fluide Produkte aus Gas – FfPaG*; Schlussbericht BMBF FKZ 033RC1301 A-G: März, 2018.
- (266) <https://www.basf.com/global/en/who-we-are/sustainability/we-produce-safely-and-efficiently/energy-and-climate-protection/carbon-management/innovations-for-a-climate-friendly-chemical-production.html> (accessed on 2021-03-18).
- (267) <https://www.basf.com/global/en/who-we-are/sustainability/we-produce-safely-and-efficiently/energy-and-climate-protection/carbon-management/interview-methane-pyrolysis.html> (accessed on 2021-03-18).
- (268) Palmer, C.; Bunyan, E.; Gelinas, J.; Gordon, M. J.; Metiu, H.; McFarland, E. W. CO₂-free hydrogen production by catalytic pyrolysis of hydrocarbon feedstocks in molten Ni–Bi. *Energy Fuels* **2020**, *34* (12), 16073–16080.
- (269) Postels, S.; Abánades, A.; von der Assen, N.; Rathnam, R. K.; Stückrad, S.; Bardow, A. Life cycle assessment of hydrogen production by thermal cracking of methane based on liquid-metal technology. *Int. J. Hydrogen Energy* **2016**, *41* (48), 23204–23212.
- (270) Dagle, R. A.; Dagle, V.; Bearden, M. D.; Holladay, J. D.; Krause, T. R.; Ahmed, S. *An overview of natural gas conversion technologies for co-production of hydrogen and value-added solid carbon products*; USDOE Office of Energy Efficiency and Renewable Energy (EERE), Transportation Office. Fuel Cell Technologies Office, 2017. DOI: 10.2172/1411934
- (271) Muradov, N. Low to near-zero CO₂ production of hydrogen from fossil fuels: Status and perspectives. *Int. J. Hydrogen Energy* **2017**, *42* (20), 14058–14088.